HYDROMAGNETIC JEFFERY-HAMEL UNSTEADY FLOW OF A DISSIPATIVE NON-NEWTONIAN FLUID WITH NONLINEAR VISCOSITY

FRANCIS OKETCH OCHIENG

MASTER OF SCIENCE IN MATHEMATICS

(Computational Option)

PAN AFRICAN UNIVERSITY

INSTITUTE FOR BASIC SCIENCES, TECHNOLOGY AND INNOVATION

2018

Hydromagnetic Jeffery-Hamel Unsteady Flow of a Dissipative Non-Newtonian Fluid with Nonlinear Viscosity

Francis Oketch OCHIENG

MC300-0001/17

A thesis submitted to the Pan African University Institute for Basic Sciences, Technology and Innovation in partial fulfillment of the requirements for the award of the degree of Master of Science in Mathematics (Computational Option) of the Pan African University

2018

Declaration

I declare that this thesis is my original work and has not been submitted to another institution for the award of a degree, diploma, or certificate.

Student's name: Francis Oketch OCHIENG

Signature:..... **Date:**.....

Declaration by Supervisors

This thesis has been submitted for examination with our approval as University Supervisors.

1. **Signature:**..... **Date:**.....

   Prof. M. Kinyanjui

   Department of Pure and Applied Mathematics

   Jomo Kenyatta University of Agriculture and Technology (JKUAT), KENYA.

2. **Signature:**..... **Date:**.....

   Dr. M. Kimathi

   Department of Mathematics and Statistics

   Machakos University (MKsU), KENYA.

Dedication

This thesis is dedicated to my parents Mr. and Mrs. Ochieng, and my siblings. You will forever remain my reasons for living.

Acknowledgements

My thanks to both the African Union Commission (AUC) and Japan International Cooperation Agency (JICA) for the financial support they extended to me in the research, authorship, and publication of this thesis. I am also obliged to my supervisors, Prof. M. Kinyanjui of Jomo Kenyatta University of Agriculture and Technology and Dr. M. Kimathi of Machakos University, for their guidance throughout the development of this thesis, especially for their insightful, constructive, and valuable comments. I also wish to thank the many authors of books, papers, and articles as well as a new generation of contributors to electronic media (the World Wide Web) who have provided me with additional insight and ideas. Lastly, I wish to recognize my parents and siblings for offering me the most needed social and spiritual support during the development of this thesis.

Table of Contents

List of Tables

List of Figures

Abbreviations and Acronyms

MHD	Magnetohydrodynamics
ODE	Ordinary Differential Equation
PDE	Partial Differential Equation
FDM	Finite Difference Method
FEM	Finite Element Method
FVM	Finite Volume Method
HPM	Homotopy Perturbation Method
HAM	Homotopy Analysis Method
DTM	Differential Transform Method
LHS	Left Hand Side
RHS	Right Hand Side
IVP	Initial Value Problem
BVP	Boundary Value Problem

Nomenclature

Roman symbols

Symbol	Meaning
$\vec{V}$	Velocity field (ms^{-1})
$\vec{E}$	Electric field (N/C)
$\vec{B}$	Magnetic field intensity ($Nm^{-1}A^{-1}$)
B_0	Constant magnetic field intensity ($Nm^{-1}A^{-1}$)
$\vec{J}$	Electric current density (Am^{-2})
$\vec{F}$	Body force (N)
n	Flow behaviour index
p	Pressure (Nm^{-2})
k	Thermal conductivity (W/mK)
m	Arbitrary constant that is related to the wedge angle
C_p	Specific heat at constant pressure (J/kg·K)
C_f	Skin-friction coefficient
g	Velocity gradient (s^{-1})
$\dot{q}_g$	Rate of heat generation per unit volume (W/m^3)
q	Charge density (Cm^{-3})
Q	Volumetric flow rate (m^3s^{-1})
x, y, z	Dimensional Cartesian coordinates
r, θ, z	Dimensional cylindrical coordinates
u_r, u_θ, u_z	Cylindrical velocity components
u_x, u_y, u_z	Cartesian velocity components
t	Time (s)
U_∞	Freestream velocity (ms^{-1})
F	Dimensionless velocity
T	Dimensional temperature (K)
T_w	Temperature of the fluid at the wall (K)
T_∞	Constant temperature of the fluid in the freestream (K)
$\frac{D}{Dt}$	Material derivative $\left(\frac{\partial}{\partial t} + \vec{V} \cdot \vec{\nabla}\right)$

Greek symbols

Symbol	Meaning
υ	Kinematic viscosity (m^2s^{-1})
ρ	Fluid density (kgm^{-3})
μ	Coefficient of dynamic viscosity (Nsm^{-2})
μ_0	Fluid consistency coefficient (Pa s^n)
μ_e	Magnetic permeability (Hm^{-1})
Ξ	Flow property/variable
$\vec{\tau}$	Shear stress vector (Nm^{-2})
$\vec{\nabla}$	Gradient operator $\left(\hat{i}\frac{\partial}{\partial x}+\hat{j}\frac{\partial}{\partial y}+\hat{k}\frac{\partial}{\partial z}\right)$
Φ	Viscous dissipation (s^2)
Ψ	Stream function
ϖ	Wedge angle
ε	Wedge angle parameter
ϵ_0	Electric permittivity
α	Thermal diffusivity (m^2s^{-1})
σ	Electrical conductivity ($\Omega^{-1}m^{-1}$)
π	Measure of the angle in radians (^{c})
θ	Wedge semi-angle ($^\circ$)
δ	Time-dependent length scale (m^{-2})
ω	Dimensionless temperature
λ	Unsteadiness parameter
γ	Friction coefficient factor
$\bar{\bar{\tau}}$	Deviatoric stress tensor
β	Coefficient of thermal expansion (K^{-1})
ξ	Magnetic permeability of free space

Dimensionless numbers

Re	Reynolds number $\left(\frac{Q\rho}{\mu_0}\right)$
Ha	Hartmann number $\left(B_0 r\left(\frac{\sigma}{\mu_0}\right)^{\frac{1}{2}}\right)$
Pr	Prandtl number $\left(\frac{\mu_0}{\rho\alpha}\right)$
Ec	Eckert number $\left(\frac{Q^2/r^2}{C_p(T_\infty - T_w)}\right)$
Nu	Nusselt number $\left(-\sqrt{\frac{Re}{(2-\epsilon)}}\omega'(0)\right)$

Abstract

The unsteady two-dimensional Jeffery-Hamel laminar flow of an incompressible non-Newtonian fluid, with nonlinear viscosity, flowing through a divergent wedge-shaped in the presence of a constant applied magnetic field in the direction perpendicular to the fluid motion has been studied. The resulting nonlinear PDEs (partial differential equations) governing this flow are reduced to a system of nonlinear ODEs (ordinary differential equations) by the similarity transformation technique. The resulting boundary value problem is solved numerically using the collocation method and simulated using MATLAB with the help of the bvp4c inbuilt function to obtain the profiles. The effects of varying the Reynolds number, Hartmann number, Prandtl number, Eckert number, and the unsteadiness parameter on the fluid velocity, fluid temperature, skin-friction coefficient, and rate of heat transfer are presented in graphs and tables; and are discussed. The results obtained indicate that there are significant effects of flow parameters on the flow variables. For instance, the effect of increasing viscous dissipation parameter (Eckert number) increases the fluid temperature which is significant in high-temperature processes such as polymer processing. This study provides useful information for engineering, technological, and industrial applications such as in hydromagnetic power generators.

Chapter 1

Introduction

A fluid refers to any substance that undergoes continuous deformation when subjected to a shearing stress of any magnitude. The shearing stress (i.e., force per unit area) is created whenever a tangential force acts on a surface. Fluid mechanics refers to the study of fluid motion and the forces that cause the motion. This study is divided into two branches, i.e., fluid kinematics and fluid dynamics.

Fluid kinematics is a branch of fluid mechanics which studies the motion of the fluid. It deals with the quantities involving space and time only (i.e., fluid velocity and acceleration) and their distribution in space.

Fluid dynamics is a branch of fluid mechanics which studies the forces that cause the motion of the fluid. These forces are classified as body forces, surface forces, and line forces. Body forces are forces which act on the fluid particles from a distance without physical contact (e.g., gravitational force, magnetic force, electrostatic force). Surface forces are the forces which are exerted on the area element by the surrounding through direct contact. They are as a result of the interaction between the fluid and its surrounding. Therefore, these forces act at the surface of the fluid element. They are directly proportional to the extent of the area and are expressed per unit area. These forces can be resolved into two components, one along the normal to an elemental area and the other along the tangential plane of the elemental area (e.g., shear forces, pressure gradient). Line forces act along a line (e.g., surface tension force).

Fluids are classified into two, incompressible and compressible fluids. A fluid is said to be incompressible if its density does not change significantly with change in pressure or temperature (i.e., the density is assumed to be constant). Otherwise, the fluid is said to be compressible.

1.1 Background of the study

The study of fluid flow through a convergent or divergent wedge-shaped has been of much interest by various researchers due to the wide range of applications in the field of engineering and technology. Mathematical formulation of viscous fluid flow in a wedge-shaped passage was pioneered by Jeffery (1915) and Hamel (1917). Therefore, this type of flow is referred to as the Jeffery-Hamel flow. Thus, Jeffery-Hamel flow refers to a convergent or divergent flow with a source or sink of fluid volume at the point of intersection of two plane walls. Figure 1.1 shows the geometry of a divergent Jeffrey-Hamel flow with a radial motion.

A non-Newtonian fluid is a fluid whose coefficient of viscosity is a variable. In practice, many fluid materials exhibit non-Newtonian fluid behavior such as: salt solutions, toothpaste, starch suspensions, paint, blood, and shampoo (Nguyen and Nguyen, 2012). It is important to note here that, many fluids of industrial importance are non-Newtonian. In real industrial applications, non-Newtonian fluids are more appropriate than Newtonian fluids due to their applications in petroleum drilling, polymer processing, certain separation processes, manufacturing of foods and paper, and some other industrial processes (Arthur et al., 2015).

The theory of magnetohydrodynamics (MHD) involves electromagnetic induction in a moving electrically conducting fluid in the presence of an applied magnetic field. Such induction exerts a force on ions of the electrically conducting fluid. The description is as follows: if an electrically conducting fluid is placed in a constant magnetic field, the motion of the fluid induces currents which create forces on the fluid. The production of these currents has led to their use in engineering and industrial applications (Manyonge et al., 2012). The theoretical study of MHD flow has been a subject of great interest due to its extensive applications in engineering processes such as in MHD power generators for electricity production, accelerators, MHD pumps, MHD flow meters, electrostatic filters, the design of cooling systems with liquid metals, and in geothermal power stations (Mukhopadhyay, 2012; Rostami et al., 2014). Considerable efforts have been made to study the MHD theory for technological application of fluid pumping system in which electrical energy forces the working of electrically conducting fluid.

Hydromagnetic Jeffery-Hamel flow has gained considerable attention due to its applications in

industrial and biological sciences. Moreover, the heat and mass transfer analysis play a vital role in the handling and processing of non-Newtonian fluids. The radiative effects have important applications in Physics and engineering processes. The radiations due to heat transfer effects on different flows are very important in space technology and high-temperature processes. Thermal radiation effects may play an important role in controlling heat transfer in polymer processing industry where the quality of the final product depends on the heat and mass controlling factors. High-temperature plasmas, cooling of nuclear reactors, and power generation systems are some important applications of radiative heat transfer (Pramanik, 2014). The consideration of MHD flow in a conduit is quite significant in crystal growth, the design of medical diagnostic devices, control of liquid metal flows, etc. Furthermore, several engineering processes such as fossil fuel combustion energy, astrophysical flows, gas turbines, solar power technology and many propulsion devices for aircraft, satellites, missiles, and space vehicle occur at high temperatures and hence thermal radiation effect becomes important. In particular, thermal radiation has a central role in engineering processes occurring at high temperature for the design of many advanced energy conversion systems and pertinent equipment (Poor et al., 2014).

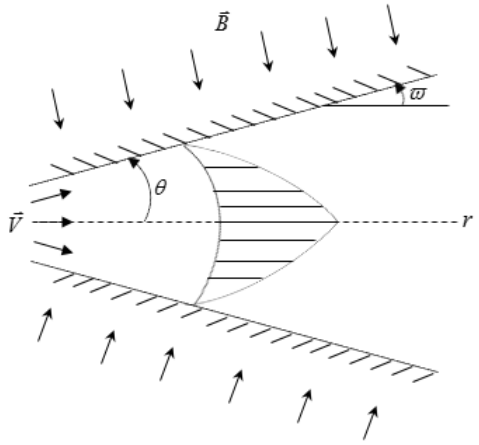

Figure 1.1: Geometry of the problem (Khan et al., 2013)

1.2 Definition of Terms

1.2.1 Wedge angle parameter

For the total angle 2ϖ of the wedge, $2\varpi = \varepsilon\pi$. The wedge angle parameter is given by

$$\varepsilon = \frac{2m}{m+1}, \tag{1.2.1}$$

where m is an arbitrary constant that is related to the wedge angle.

1.2.2 Power law model

This model is also known as Ostwald-de Waele model. Power-law fluid is a type of generalized Newtonian fluid for which the shear stress, τ, is given by

$$\tau = \mu_0 \left(\frac{du}{dy}\right)^{n-1} \frac{du}{dy}, \tag{1.2.2}$$

where $\dfrac{du}{dy}$ is the shear rate (or velocity gradient) perpendicular to the plane of shear, μ_0 is the fluid consistency coefficient, and n is the flow behaviour index. Equation (1.2.2) is useful because of its simplicity but only approximately describes the behaviour of a real non-Newtonian fluid.

The quantity

$$\mu = \mu_0 \left(\frac{du}{dy}\right)^{n-1} \tag{1.2.3}$$

represents an apparent viscosity as a function of the shear rate (SI unit Pa s). Power-law fluids can be classified into either Newtonian or non-Newtonian based on the value of their flow behavior index, n. If $n = 1$, then the fluid is said to be Newtonian since the viscosity is a constant. If otherwise, the fluid is said to be non-Newtonian. Non-Newtonian fluids can further be classified into two categories: pseudoplastic and dilatant. A fluid in which $n < 1$ is called pseudoplastic, i.e., the fluid exhibits shear-thinning properties (e.g., blood, milk) while a fluid in which $n > 1$ is called dilatant, i.e., the fluid shows shear-thickening behavior (e.g., sugar solution). The present study is devoted to a dilatant.

1.2.3 Laminar and Turbulent flow

Fluid flow is said to be laminar if the paths followed by the fluid particles as they move do not cross one another (i.e., the particles move in layers). In turbulent flow, the particles moves in a zigzag way. Laminar and turbulent flows are characterized by the value of the Reynolds number which is defined as the ratio of inertia force to the viscous force.

1.2.4 Steady and Unsteady flow

Fluid flow is said to be unsteady if all the flow variables (e.g., velocity, pressure, temperature) depend on time (i.e., $\frac{\partial \Xi}{\partial t} \neq 0$). If the fluid properties at a point in the system do not change over time, the flow is said to be steady (i.e., $\frac{\partial \Xi}{\partial t} = 0$).

The present study considers an unsteady flow. A constant unsteadiness parameter, λ, is usually introduced in the equations governing the unsteady flow of fluids in order to account for the time factor. According to Rahman et al. (2016), this parameter is defined as follows:

$$\lambda = \frac{\rho \delta^m}{\mu r^{m-1}} \frac{d\delta}{dt}, \tag{1.2.4}$$

where δ represents the time-dependent length scale, m is an arbitrary constant that is related to the wedge semi-angle, and r is the radial distance. This parameter makes the governing equations locally similar. It is noted that $\lambda = 0$ implies that the flow is steady.

1.2.5 Magnetohydrodynamics

The word magnetohydrodynamics (MHD) comprises of the words *magneto*- meaning magnetic, *hydro*- meaning liquid, and *dynamics*- meaning the movement of an entity when subjected to some forces. Thus MHD is a branch of science that deals with the study of the motion of fluid when a magnetic field is applied. It is also referred to as hydromagnetics. The interaction between electric and magnetic fields is referred to as electromagnetism.

If an electrically conducting fluid (e.g., plasma, liquid metals) flows in presence of a magnetic field, there arises an interaction between the flow field and the magnetic field. The magnetic field exerts

a force (i.e., mechanical force) on the fluid due to the induced electric current. The induced electric current, in turn, produces an induced magnetic field. Thus, the original magnetic field is changed. There develops a component of an electric field in the direction perpendicular to both the flow field and the magnetic field. The phenomenon which involves the production of a potential difference across a moving electrically conducting fluid when a magnetic field is applied in a direction perpendicular to the electric current is referred to as Hall effect.

1.2.6 Boundary layer

A boundary layer is a thin region in the fluid adjacent to the boundary where the effects of viscosity are significant. In this layer, the viscous force dominates over the inertial force. A range of velocities exist across the boundary layer from maximum to zero, provided the fluid is in contact with the boundary.

1.2.7 Viscous dissipation

Viscosity refers to a measure of fluid resistance to gradual deformation by shear stress. Viscosity in liquids decreases with an increase in fluid temperature. This is because as the temperature increases, the cohesive forces reduce and as a result, making the liquid to be less viscous. In a viscous fluid flow, the viscosity of the fluid absorbs kinetic energy from the motion of the fluid and converts it into heat (i.e., the internal energy of the fluid). This heats up the fluid. Therefore, this process is referred to as viscous dissipation.

1.2.8 Heat transfer

Heat transfer is the study of kinetic energy transfer that takes place between bodies due to the temperature difference. The temperature difference may be as a result of a fluid dissipating heat or introduction of heat to the flow field. If there exists a temperature difference, then the study of heat transfer is necessary. Heat transfer can take place either by conduction, radiation, or convection.

1.2.8.1 Conduction

Conduction is the mode of heat transfer that takes place when a temperature gradient exists in a stationary medium, which may be a solid or fluid.

1.2.8.2 Convection

Convection is the mode of heat transfer that takes place from one place to another by the movement of fluids at different temperatures. The motion of the fluid is as a result of imbalance on the forces acting on the fluid particles. Convective heat transfer may be categorized according to the nature of the flow (i.e., free and forced convection). Free (or natural) convection is the mode of heat transfer in which the flow is as a result of density gradient created by temperature variation. On the other hand, forced convection occurs when the flow is caused by some external means. The present study considers free convective heat transfer.

1.2.8.3 Radiation

Radiation is the mode of heat transfer in which there is a net heat transmission due to electromagnetic wave propagation that takes place in a vacuum.

1.2.9 Some important parameters of engineering interest

They include the skin-friction coefficient and the wall heat transfer rate. These are discussed below according to Rahman et al. (2016).

1.2.9.1 Nusselt number

Nusselt number, Nu, is a dimensionless number defined as the ratio of convective to conductive heat transfer across (perpendicular to) the boundary (Batchelor, 2000). It can be expressed as follows:

$$N_u = \frac{\text{convective heat transfer}}{\text{conductive heat transfer}}.$$

Convective heat transfer relationships are usually expressed in terms of Nusselt number as a function of Reynolds Number and Prandtl Number. The Nusselt number is directly proportional to the negative of the temperature gradient.

The Nusselt number can be negative since it is defined as the dimensionless temperature gradient at the wall. The slope may be negative or positive, depending on the direction of heat flux.

1.2.9.2 Skin-friction coefficient

Skin-friction refers to a drag (or resistance to motion) created by the fluid particles rubbing against the wall. The boundary layer formed produces a drag which is exerted on the wall of the wedge due to the viscous stresses which are developed at the wall. The skin-friction coefficient is very important for engineers since it enables them to determine the material (or coating) to use in order to construct materials which preserve energy. The skin-friction coefficient is directly proportional to the velocity gradient (Batchelor, 2000).

1.3 Problem statement

Fluid flow is usually unsteady and takes place in the presence of both surface forces (e.g., shear forces) and body forces (e.g., gravity, electromagnetic force). These forces may either accelerate or retard the motion of the fluid. The previous studies on Jeffery-Hamel flow have focused on steady flow in the presence of body forces. Some existing studies, however, have investigated the unsteady Jeffery-Hamel flow but neglected the effect of body forces. For instance, Nagler (2017) studied the steady Jeffery-Hamel flow inside a convergent wedge but assumed that the body forces are negligible. The study of steady flow may not provide adequate information for engineers since the steady flow is independent of time. Furthermore, assuming that the body forces are negligible in fluid flow means that some vital pieces of information of engineering interest are lacking. Therefore, the present study aims to extend the work of Nagler (2017) by investigating the unsteady Jeffery-Hamel flow inside a divergent wedge in the presence of a magnetic field which will act as the body force.

1.4 Justification of the study

This study is necessary because fluid flows are usually unsteady in nature and take place in the presence of both surface forces (such as pressure gradient and viscous forces) and body forces (such as gravity and electromagnetic forces). Many fluids of industrial importance are non-Newtonian due to their wide range of applications in industrial processes. A constant magnetic field is introduced in the flow field since MHD flow has various important applications across a multitude of fields. For instance, MHD flow is useful in designing communication systems, MHD power generating systems, MHD accelerators, etc., and in medicine such as Magnetic Drug Targeting in cancer therapy.

1.5 Objectives of the study

The following are the objectives of this study:

1.5.1 General objective

To study the unsteady Jeffery-Hamel flow of an incompressible non-Newtonian fluid with nonlinear viscosity in the presence of an applied magnetic field in the direction perpendicular to the fluid motion.

1.5.2 Specific objectives

1. To model the unsteady Jeffery-Hamel flow of an incompressible non-Newtonian fluid with nonlinear viscosity in the presence of an applied magnetic field in the direction perpendicular to the fluid motion.
2. To investigate the effects of the flow parameters on velocity, temperature, skin-friction, and rate of heat transfer.
3. To compute the skin-friction coefficient and the rate of heat transfer.

1.6 Significance of the Study

This study provides useful information for engineers, i.e., the data on the skin-friction coefficient and the rate of heat transfer. Such information is vital for engineering and industrial applications such as in the design of MHD power generating systems, communication and radar systems, MHD accelerators, electrostatic filters, heat exchangers, medical diagnostic devices, in polymer processing, and in the cooling of nuclear reactors.

1.7 Scope of the study

This study is limited to the unsteady, two-dimensional, laminar flow of an incompressible electrically conducting non-Newtonian fluid with viscous dissipation. The fluid is confined inside a divergent wedge-shaped subjected to a constant applied magnetic field in the direction perpendicular to the fluid motion. The study assumes a symmetrical flow that is purely radial (i.e., the motion is such that

there is no change in the flow variable along the z-direction) and that the perpendicular and tangential velocities are negligible.

The rest of the thesis is organized as follows: Chapter 2 presents the literature related to and necessary for the present study, Chapter 3 presents the model formulation and mathematical analysis, Chapter 4 presents the numerical simulations of the corresponding model, Chapter 5 presents the results of the study, Chapter 6 presents the conclusion of the study and recommendations for future studies, and section A.1 presents the publication of this study.

Chapter 2

Literature Review

2.1 Overview

This chapter reassesses some studies that are relevant to the present study. Thus, this chapter is primarily devoted to a brief literature review of the recent investigations made on the MHD Jeffery-Hamel flow.

2.2 Literature Review

Hydromagnetic Jeffery-Hamel flow of non-Newtonian fluids has been studied and discussed extensively by many authors. Domairry et al. (2009) found analytically that velocity distributions are very different for convergent and divergent wedge-shaped in the case of a steady two-dimensional flow of an incompressible conducting viscous fluid from a source (or a sink) at the intersection between two rigid plane walls. The study assumed that the velocity is along the radial direction and dependent on r and θ only. Moreover, the study found that in the convergent wedge-shaped, for large Reynolds number, the velocity is almost constant for a large section in the center and only close to the walls it drops off sharply to zero.

In the study of the unsteady two-dimensional flow of a MHD non-Newtonian Maxwell fluid over a stretching surface with a prescribed surface temperature in the presence of a heat source or sink, Imani et al. (2012) found numerically that fluid velocity initially decreases with the increasing unsteadiness parameter, and temperature decreases significantly due to unsteadiness. Further, the study found numerically that the fluid velocity decreases with the increasing magnetic parameter. Increasing the Maxwell parameter values has the effect of suppressing the velocity field and increasing the temperature. In the study, the study assumed that the magnetic Reynolds number is very small and that the electric field due to the polarization of charges is negligible. Mukhopadhyay (2012) studied the effects of magnetic field and nanoparticle on the Jeffery-Hamel flow of fluid through a divergent wedge-shaped. He analytically found that the rate of transport is considerably

reduced with an increase in Hartmann number. This clearly indicates that the transverse magnetic field opposes the transport phenomena.

Hasanpour et al. (2011) carried out a study of the momentum, free convection heat and mass transfer of a MHD flow over a movable permeable plumb surface. The study considered the case of a steady, incompressible, two-dimensional MHD flow with free convection on a movable leaky vertical surface and found that the momentum, heat and mass transfer phenomena depend on the magnetic parameter, Prandtl number, Schmidt number, buoyancy ratio and suction or blowing parameter. The external magnetic field reduces the velocity value and consequently the flow rate and also the wall heat transfer. An increase in the value of the Hartman number and buoyancy ratio results in a decrease in the velocity profile. The temperature value is decreased when the magnitude of the suction parameter and blowing parameter increase. Also, the concentration magnitude decreases when the Schmidt number increases.

Mukhopadhyay et al. (2013) studied the unsteady two-dimensional flow of Casson fluid over a stretching surface having a prescribed surface temperature and found numerically that fluid velocity initially decreases with increasing unsteadiness parameter and temperature decreases significantly due to unsteadiness. The effect of increasing values of the Casson parameter suppresses the velocity field but the temperature is enhanced with increasing Casson parameter. Domairry et al. (2009) studied Jeffery-Hamel flow and concluded that the velocity increases with an increase in the wedge opening semi-angle for the case of diverging wedge-shaped; the influence of Reynolds number Re and the wedge opening semi-angle is same for diverging wedge-shaped; there is an increase in the velocity for converging wedge-shaped with an increase in wedge opening semi-angle; For converging wedge-shaped, Reynolds number Re results in an increase in the velocity which is opposite to that for diverging wedge-shaped.

Pramanik (2014) studied the Casson fluid flow and heat transfer past an exponentially porous stretching surface in presence of thermal radiation and numerically found that the effect of suction parameter on a viscous incompressible fluid suppresses the velocity field which in turn causes the enhancement of skin-friction coefficient; skin-friction coefficient is higher for suction than that of blowing; thermal radiation enhances the effective thermal diffusivity and the temperature increases with increasing values of the radiation parameter. Poor et al. (2014) studied the effects of thermal radiation in a two-dimensional and magnetohydrodynamic (MHD) flow of an incompressible

non-Newtonian fluid in a convergent/divergent wedge-shaped and observed that the temperature is a decreasing function of thermal radiation.

Arthur et al. (2015) studied the casson fluid flow over a vertical porous surface with chemical reaction in the presence of a transverse magnetic field and found that the combined effect of magnetic field, Casson parameter, Schmidt number, reaction rate parameter and suction parameter increase the local skin friction; whereas that of the buoyancy force decreases the local skin friction at the surface of the plate. The study found further that the combined effect of magnetic parameter and suction parameter is to decrease the velocity of the fluid. This is due to the fact that the transverse magnetic field induces a Lorentz force which tends to provide resistance to the fluid flow.

In the study of MHD Jeffery–Hamel Nanofluid Flow in Non-Parallel Walls, Sheikholeslami et al. (2015) found semi-analytically that the velocity boundary layer thickness decreases with increasing Reynolds number and nanoparticle volume fraction and increases with increasing Hartmann number. The study found further that an increase in Reynolds number leads to an increase in the magnitude of the skin-friction coefficient. Generally, when the magnetic field is imposed on the wedge, the velocity field is suppressed owing to the retarding effect of the Lorenz force. Thus, the presence of the magnetic field increases the momentum boundary layer thickness. The study found that the skin-friction coefficient is an increasing function of Reynolds number, opening angle and nanoparticle volume friction but a decreasing function of Hartmann number.

Ananthaswamy and Yogeswari (2016) studied the MHD Jeffery-Hamel flow in nanofluids using new homotopy analysis method and found that an increase in Hartmann number increases the fluid velocity while an increase in Reynolds number decreases the fluid velocity for both viscous and nanofluid. Mohyud-Din et al. (2016) studied magnetohydrodynamic flow and heat transfer of copper–water nanofluid in a wedge-shaped with non-parallel walls considering different shapes of nanoparticles and found numerically that an increase in wedge opening and the Reynolds number results in backflow for diverging wedge-shaped case. This backflow can be reduced by employing a strong magnetic field. Moreover, the magnetic number increases the velocity of the fluid. Khan et al. (2016) studied the Jeffery-Hamel flow of a non-Newtonian fluid and found that for a diverging wedge-shaped, an increase in wedge opening semi-angle and Reynolds number results to a decrease in the fluid velocity. For all these parameters, the maximum velocity is observed near the center of

the wedge-shaped channel.

Nagler (2017) studied the Jeffery-Hamel flow of non-Newtonian fluid with nonlinear viscosity and wall friction and found that: the Newtonian normalized velocity gradually decreases with the tangential direction progress, an increase in the friction coefficient leads to a decrease in the normalized Newtonian velocity profile values, and an increase in the Reynolds number results to an increase in the normalized velocity function values.

From the cited studies above, unsteady Jeffery-Hamel flow of a dissipative non-Newtonian fluid with nonlinear viscosity has received little attention. A lot of emphasis should be laid on the unsteadiness, variable viscosity, and effects of body forces for a model to adequately describe fluid flow and provide vital pieces of information of engineering interest. Therefore, the present study aims to extend the previous work of Nagler (2017) by investigating the unsteady two-dimensional Jeffery-Hamel flow of an incompressible non-Newtonian fluid with nonlinear viscosity inside a divergent wedge-shaped in the presence of an applied magnetic field.

The next chapter presents the mathematical modeling of the problem in the present study.

Chapter 3

Governing Equations and Mathematical Modeling

3.1 Overview

This chapter describes the mathematical model for the physical problem. However, many physical phenomena provide challenges when developing the corresponding mathematical models. So, it is intuitive to make some meaningful assumptions to reduce the problem into a solvable one. First, the general physical equations are developed, the equations are reduced by making some assumptions, and finally a similarity transformation technique is adopted to trim down the complexity of the formulation. The final set of the model equations for the current problem are then set up.

3.2 Problem formulation

This study considers a viscous fluid flow in a divergent wedge-shaped as shown in Figure 1.1. The fluid is electrically conducting and the effect of pressure on the fluid density is negligible. The partial derivatives with respect to z vanish since the flow field is infinite in extent in the z-direction (i.e., the flow is unbounded in the z-direction or that the z-direction is too long). A coordinate system is chosen with the origin at the center of the wedge as shown in Figure 1.1. The z-direction is taken to be the length of the wedge and r-direction is taken to be the coordinate axis perpendicular to the wall. In order to reduce complexity and achieve the outlined objectives in chapter 1, the following assumptions are made.

3.3 Assumptions

When developing a mathematical model for natural phenomena, some meaningful assumptions can be made to reduce the complexity of the problem. The following assumptions are considered in the model formulation.

1. The fluid is incompressible and electrically conducting.

2. The fluid is dissipative (i.e., the source of energy is from viscous dissipation).
3. The flow is two-dimensional and laminar.
4. The flow is unbounded in the z-direction and both the tangential and perpendicular velocities are negligible.
5. There is no chemical reaction taking place in the fluid.
6. The thermal conductivity k is a constant.
7. The induced magnetic field is negligible in the flow field in comparison with the applied magnetic field.
8. There is no external electric field applied, so the effect of polarization of the fluid is negligible.
9. The flow is non-relativistic.

3.4 Governing equations

The fundamental equations of fluid dynamics are based on the following universal laws of conservation: conservation of mass, conservation of momentum, and conservation of energy. The following are the equations governing the fluid flow in the present study.

3.4.1 Equation of continuity

This is derived from the principle of conservation of mass. The general form of continuity equation, in vector notation, for a compressible fluid flow is given by

$$\frac{\partial \rho}{\partial t} + \vec{\nabla} \cdot (\rho \vec{V}) = 0. \tag{3.4.1}$$

Equation (3.4.1) is based on two fundamental principles. The first principle states that under normal conditions, the fluid mass is neither created nor destroyed (i.e., the mass is conserved). The second principle states that there are no empty spaces between particles that are in contact and that the fluid volume is not affected by an increase in pressure (i.e., the flow is continuous). This is also referred to as the continuum hypothesis.

The present study considers cylindrical coordinates (r, θ, z) where r is measured from the axis of the wedge, θ from some convenient meridian plane, and z along the axis of the wedge. Therefore, writing equation (3.4.1) in cylindrical coordinates yields

$$\frac{\partial \rho}{\partial t} + \left(\frac{1}{r}\frac{\partial (r)}{\partial r}\hat{r} + \frac{1}{r}\frac{\partial}{\partial \theta}\hat{\theta} + \frac{\partial}{\partial z}\hat{k}\right) \cdot (u_r\hat{r} + u_\theta\hat{\theta} + u_z\hat{k})\rho = 0, \;\; r \neq 0. \tag{3.4.2}$$

Since an incompressible fluid is considered, it means that the density of the fluid is assumed to be a constant. Thus, there is no change in the fluid density. Therefore, $\dfrac{\partial \rho}{\partial t} = 0$.

Thus, equation (3.4.2) reduces to

$$\begin{aligned} \left(\frac{1}{r}\frac{\partial (r)}{\partial r}\hat{r} + \frac{1}{r}\frac{\partial}{\partial \theta}\hat{\theta} + \frac{\partial}{\partial z}\hat{k}\right) \cdot (u_r\hat{r} + u_\theta\hat{\theta} + u_z\hat{k}) = 0, \;\; r \neq 0 \\ \Rightarrow \frac{1}{r}\frac{\partial (ru_r)}{\partial r} + \frac{1}{r}\frac{\partial u_\theta}{\partial \theta} + \frac{\partial u_z}{\partial z} = 0. \end{aligned} \tag{3.4.3}$$

Since both the tangential and perpendicular velocities are negligible, equation (3.4.3) reduces to

$$\frac{\partial}{\partial r}(ru_r) = 0. \tag{3.4.4}$$

Equation (3.4.4) represents the continuity equation in cylindrical coordinates for an unsteady two-dimensional laminar flow of an incompressible fluid whose motion is assumed to be symmetrical and purely radial.

3.4.2 Equations of electromagnetism

The electromagnetic equations for formulating the MHD phenomenon are Maxwell's equation and Ohm's law. The following is a brief discussion of these equations.

3.4.2.1 Maxwell's equations

To analyze and describe the action of charged particles on each other, the concept of a point charge is useful. The physical conservation laws of electric charge and equations of electrical current density

are required in describing MHD phenomenon mathematically. The Maxwell's equations of electromagnetism relate the electric field $\vec{E}$, magnetic field $\vec{B}$, electric current density $\vec{J}$, and the electric charge density q independently on the properties of the matter (Mutua, 2013). The Maxwell's equations for time-dependent electromagnetic fields are expressed as

$$\vec{\nabla} \times \vec{E} = -\frac{\partial \vec{B}}{\partial t}, \tag{3.4.5}$$

$$\vec{\nabla} \times \vec{B} = \xi \left(\vec{J} + \epsilon_0 \frac{\partial \vec{E}}{\partial t} \right), \tag{3.4.6}$$

$$\vec{\nabla} \cdot \vec{B} = 0, \tag{3.4.7}$$

and

$$\vec{\nabla} \cdot \vec{E} = \frac{q}{\epsilon_0}. \tag{3.4.8}$$

Equations (3.4.5), (3.4.6), and (3.4.8) are referred to as Faraday's law, Ampere's law, and Gauss's law, respectively. The Faraday's law expresses the postulate for electromagnetic induction which asserts that the electric field intensity in a region of time-dependent magnetic flux density is non-conservative and cannot be expressed as a gradient or scalar potential.

This study is limited to an electrically conducting fluid in the presence of an applied magnetic field in the direction perpendicular to the fluid motion. Furthermore, it is assumed that there is no electromagnetic induction and that the field strength is constant. According to Manyonge et al. (2012), the MHD phenomenon can be described as follows: consider an electrically conducting fluid moving with velocity $\vec{V}$. The magnetic field is applied in the direction perpendicular to the fluid motion. The magnitude of the magnetic field is represented by the vector $\vec{B}$.

3.4.2.2 Equation of electrical current density (Ohm's law)

Ohm's law is a characteristic feature of the ability of the fluid to transport electric charge under the influence of an applied magnetic field. A conductive fluid moving with the velocity $\vec{V}$ in the presence of a magnetic field of strength $\vec{B}$ is considered. The relative motion induces an electric current which exerts an electric force on the charged particles giving rise to an electric current density $\vec{J}$. Current density is a measure of the density of an electric current. It is defined as a vector whose magnitude is the electric current per unit cross-sectional area. The current and current density are related by

$$I = \int \vec{J} \cdot \mathrm{d}\vec{A},$$

where $\mathrm{d}\vec{A}$ is the differential cross-sectional area vector.

The Hall effect is the production of a voltage difference (the Hall voltage) across an electrical conductor, transverse to an electric current in the conductor and to an applied magnetic field perpendicular to the current (Shah et al., 2017). The Hall effect is due to the nature of the current in an electric conductor. Current consists of the movement of many small charge carriers, typically electrons, holes, and ions. When a magnetic field is present, these charges experience a force, called the Lorentz force. When such a magnetic field is absent, the charges follow approximately straight, 'line of sight' paths between collisions with impurities, phonons, etc. However, when a magnetic field with a perpendicular component is applied, their paths between collisions are curved, thus moving charges accumulate on one face of the material. This leaves equal and opposite charges exposed on the other face, where there is a scarcity of mobile charges. The result is an asymmetric distribution of charge density across the Hall element, arising from a force that is perpendicular to both the 'line of sight' path and the applied magnetic field. The separation of charge establishes an electric field that opposes the migration of further charge, so a steady electric potential is established for as long as the charge is flowing.

Therefore, if an electric current flows through a conductor in a magnetic field, the magnetic field exerts a transverse force on the moving charge carriers which tends to push them to one side of the conductor. A buildup of charge at the sides of the conductors will balance this magnetic influence, producing a measurable voltage between the two sides of the conductor. The presence of this measurable transverse

voltage is called the Hall effect as shown in Figure 3.1. The Hall effect can be used to measure magnetic fields with a Hall probe.

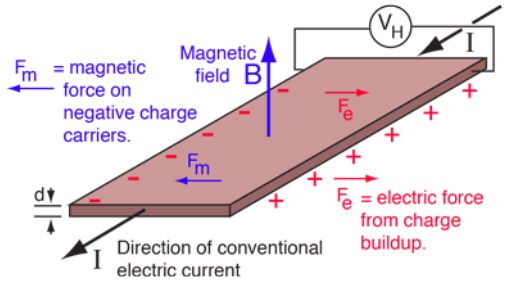

Figure 3.1: Hall effect (Yang, 2008)

Without considering the Hall effect, then by Ohm's law the electric current density induced in the conductive fluid is given by

$$\vec{J} = \sigma\left(\vec{E} + \vec{V} \times \vec{B}\right). \tag{3.4.9}$$

Since there is no external electric field (i.e., $\vec{E} = 0$), equation (3.4.9) reduces to

$$\vec{J} = \sigma\left(\vec{V} \times \vec{B}\right). \tag{3.4.10}$$

Equation (3.4.10) represents the equation of electrical current density for a conductive fluid moving at velocity $\vec{V}$ in presence of an applied magnetic field of magnitude $\vec{B}$.

In addition to the induced electric current, there is the Lorentz force $\vec{F}$ (i.e., total electromagnetic force) given by $\vec{F} = \frac{1}{\rho}\left(\rho_e\vec{E} + \vec{J} \times \vec{B}\right)$. In the current problem, the electrostatic force $\rho_e\vec{E}$ is negligibly small as compared to the electromagnetic force $\vec{J} \times \vec{B}$ since there is no externally applied electric current. Hence,

$$\vec{F} = \frac{1}{\rho}\left(\vec{J} \times \vec{B}\right) = \frac{\sigma}{\rho}\left((\vec{V} \times \vec{B}) \times \vec{B}\right). \tag{3.4.11}$$

This Lorentz force occurs because as an electric generator, the conducting fluid cuts the lines of the magnetic field.

The unsteady flow of an electrically conducting, viscous, incompressible fluid through a divergent wedge-shaped in the presence of an applied magnetic field, whose strength is constant, in the direction perpendicular to the fluid motion is considered. From vector analysis, the product of any three vectors $\vec{A}, \vec{B}$, and $\vec{C}$ is given by

$$(\vec{B} \times \vec{C}) \times \vec{A} = -\vec{A} \times (\vec{B} \times \vec{C}) = -\Big[(\vec{A} \cdot \vec{C})\vec{B} - (\vec{A} \cdot \vec{B})\vec{C}\Big]. \tag{3.4.12}$$

Thus, equation (3.4.11) becomes:

$$\vec{F} = \frac{\sigma}{\rho}\Big((\vec{V} \times \vec{B}) \times \vec{B}\Big) = -\frac{\sigma}{\rho}\Big(\vec{B} \times (\vec{V} \times \vec{B})\Big) = -\frac{\sigma}{\rho}\Big[[\vec{B} \cdot \vec{B}]\vec{V} - [\vec{B} \cdot \vec{V}]\vec{B}\Big]. \tag{3.4.13}$$

Since the magnetic field is applied in a direction perpendicular to the fluid motion, $\vec{B} \cdot \vec{V} = 0$. Furthermore, it is assumed that $\vec{B} = (B_0, 0, 0)$ and $\vec{V} = (u_r, 0, 0)$. Thus, the body force $\vec{F}$ becomes:

$$\vec{F} = -\frac{\sigma}{\rho}\Big[[\vec{B} \cdot \vec{B}]\vec{V}\Big] = -\frac{\sigma}{\rho}B_0^2 u_r \hat{r}. \tag{3.4.14}$$

3.4.3 Equation of conservation of momentum

This is derived from the principle of conservation of momentum. It is derived from Newton's second law of motion which states that the rate of change of momentum of a body is equal to the resultant force acting on the body. The momentum of a body is defined as the product of its mass and velocity. Thus, when a force is applied to an incompressible fluid of any given mass its velocity changes. The general equation of motion, in vector notation, for an incompressible fluid flow is given by:

$$\rho\frac{D\vec{V}}{Dt} = -\vec{\nabla}p - \vec{\nabla} \cdot \vec{\tau} + \rho\vec{F}, \tag{3.4.15}$$

where the stress vector $\vec{\tau}$ represents six shear stresses (i.e., stresses acting in the direction of flow) and three normal stresses (i.e., compressive or tensile stresses perpendicular to the direction of the flow).

Generally, if both the gravity and magnetic force affect the flow, the net body force is given by

$$\rho\vec{F} = \rho\vec{g} + \vec{J} \times \vec{B}. \tag{3.4.16}$$

Since the gravitational force is negligible (i.e., $\rho\vec{g} = 0$), equation (3.4.16) becomes:

$$\rho\vec{F} = \vec{J} \times \vec{B}. \tag{3.4.17}$$

Thus, equation (3.4.17) is the expression for the body force. The expression for equation (3.4.17) is as shown in equation (3.4.14). The operator $\dfrac{D}{Dt}$ is known as the material derivative. It is defined by $\dfrac{D}{Dt} = \dfrac{\partial}{\partial t} + \vec{V} \cdot \vec{\nabla}$.

Therefore, equation (3.4.15) becomes:

$$\rho\Big(\frac{\partial \vec{V}}{\partial t} + \vec{V} \cdot \vec{\nabla}\vec{V}\Big) = -\vec{\nabla}p - \vec{\nabla} \cdot \vec{\tau} + \rho\vec{F}. \tag{3.4.18}$$

The stress form of equation (3.4.18) in cylindrical coordinates is given by Salih (2011) as follows:

$$\begin{aligned}
&\hat{r}\text{-component:} && \rho\Big(\frac{\partial u_r}{\partial t} + u_r\frac{\partial u_r}{\partial r} + \frac{u_\theta}{r}\frac{\partial u_r}{\partial \theta} + u_z\frac{\partial u_r}{\partial z} - \frac{u_\theta^2}{r}\Big) = -\frac{\partial p}{\partial r} \\
&&& \quad + \frac{1}{r}\frac{\partial}{\partial r}(r\tau_{rr}) + \frac{1}{r}\frac{\partial \tau_{r\theta}}{\partial \theta} + \frac{\partial \tau_{rz}}{\partial z} - \frac{\tau_{\theta\theta}}{r} + \rho F_r \\
&\hat{\theta}\text{-component:} && \rho\Big(\frac{\partial u_\theta}{\partial t} + u_r\frac{\partial u_\theta}{\partial r} + \frac{u_\theta}{r}\frac{\partial u_\theta}{\partial \theta} + u_z\frac{\partial u_\theta}{\partial z} + \frac{u_r u_\theta}{r}\Big) = -\frac{1}{r}\frac{\partial p}{\partial \theta} \\
&&& \quad + \frac{1}{r^2}\frac{\partial}{\partial r}(r^2\tau_{\theta r}) + \frac{1}{r}\frac{\partial \tau_{\theta\theta}}{\partial \theta} + \frac{\partial \tau_{\theta z}}{\partial z} + \rho F_\theta \\
&\hat{k}\text{-component:} && \rho\Big(\frac{\partial u_z}{\partial t} + u_r\frac{\partial u_z}{\partial r} + \frac{u_\theta}{r}\frac{\partial u_z}{\partial \theta} + u_z\frac{\partial u_z}{\partial z}\Big) = -\frac{\partial p}{\partial z} + \frac{1}{r}\frac{\partial}{\partial r}(r\tau_{zr}) + \frac{1}{r}\frac{\partial \tau_{z\theta}}{\partial \theta} + \frac{\partial \tau_{zz}}{\partial z} + \rho F_z.
\end{aligned} \tag{3.4.19}$$

F_r, F_θ and F_z are the components of the body force per unit mass of the fluid in the r, θ and z direction, respectively. Since the flow is unbounded in the z-direction and both the tangential and perpendicular velocities are negligible so equations (3.4.19) reduce to

$$\begin{aligned}
&\hat{r}\text{-component:} && \rho\Big(\frac{\partial u_r}{\partial t} + u_r\frac{\partial u_r}{\partial r}\Big) = -\frac{\partial p}{\partial r} + \frac{1}{r}\frac{\partial}{\partial r}(r\tau_{rr}) + \frac{1}{r}\frac{\partial \tau_{r\theta}}{\partial \theta} - \frac{\tau_{\theta\theta}}{r} + \rho F_r \\
&\hat{\theta}\text{-component:} && 0 = -\frac{1}{r}\frac{\partial p}{\partial \theta} + \frac{1}{r^2}\frac{\partial}{\partial r}(r^2\tau_{\theta r}) + \frac{1}{r}\frac{\partial \tau_{\theta\theta}}{\partial \theta} + \rho F_\theta.
\end{aligned} \tag{3.4.20}$$

According to Salih (2011) and Nagler (2017), the following stress matrix gives the expressions for the shear stress components and the normal stress components in cylindrical coordinates:

$$\begin{pmatrix} \tau_{rr} & \tau_{r\theta} & \tau_{rz} \\ \tau_{\theta r} & \tau_{\theta\theta} & \tau_{\theta z} \\ \tau_{zr} & \tau_{z\theta} & \tau_{zz} \end{pmatrix} = \mu \begin{pmatrix} 2\dfrac{\partial u_r}{\partial r} - \dfrac{2}{3}\vec{\nabla}\cdot\vec{V} & \dfrac{1}{r}\dfrac{\partial u_r}{\partial \theta} + \dfrac{\partial u_\theta}{\partial r} - \dfrac{u_\theta}{r} & \dfrac{\partial u_z}{\partial r} + \dfrac{\partial u_r}{\partial z} \\ \dfrac{1}{r}\dfrac{\partial u_r}{\partial \theta} + \dfrac{\partial u_\theta}{\partial r} - \dfrac{u_\theta}{r} & 2\Big(\dfrac{1}{r}\dfrac{\partial u_\theta}{\partial \theta} + \dfrac{u_r}{r}\Big) - \dfrac{2}{3}\vec{\nabla}\cdot\vec{V} & \dfrac{\partial u_\theta}{\partial z} + \dfrac{1}{r}\dfrac{\partial u_z}{\partial \theta} \\ \dfrac{\partial u_z}{\partial r} + \dfrac{\partial u_r}{\partial z} & \dfrac{\partial u_\theta}{\partial z} + \dfrac{1}{r}\dfrac{\partial u_z}{\partial \theta} & 2\dfrac{\partial u_z}{\partial z} - \dfrac{2}{3}\vec{\nabla}\cdot\vec{V} \end{pmatrix} \quad (3.4.21)$$

Since the fluid is incompressible, $\vec{\nabla}\cdot\vec{V} = 0$. Thus, the matrix (3.4.21) reduces to

$$\begin{pmatrix} \tau_{rr} & \tau_{r\theta} & \tau_{rz} \\ \tau_{\theta r} & \tau_{\theta\theta} & \tau_{\theta z} \\ \tau_{zr} & \tau_{z\theta} & \tau_{zz} \end{pmatrix} = \mu \begin{pmatrix} 2\dfrac{\partial u_r}{\partial r} & \dfrac{1}{r}\dfrac{\partial u_r}{\partial \theta} + \dfrac{\partial u_\theta}{\partial r} - \dfrac{u_\theta}{r} & \dfrac{\partial u_z}{\partial r} + \dfrac{\partial u_r}{\partial z} \\ \dfrac{1}{r}\dfrac{\partial u_r}{\partial \theta} + \dfrac{\partial u_\theta}{\partial r} - \dfrac{u_\theta}{r} & 2\Big(\dfrac{1}{r}\dfrac{\partial u_\theta}{\partial \theta} + \dfrac{u_r}{r}\Big) & \dfrac{\partial u_\theta}{\partial z} + \dfrac{1}{r}\dfrac{\partial u_z}{\partial \theta} \\ \dfrac{\partial u_z}{\partial r} + \dfrac{\partial u_r}{\partial z} & \dfrac{\partial u_\theta}{\partial z} + \dfrac{1}{r}\dfrac{\partial u_z}{\partial \theta} & 2\dfrac{\partial u_z}{\partial z} \end{pmatrix} \quad (3.4.22)$$

Since the flow is unbounded in the z-direction and both the tangential and perpendicular velocities are negligible, the matrix (3.4.22) reduces to

$$\begin{pmatrix} \tau_{rr} & \tau_{r\theta} & \tau_{rz} \\ \tau_{\theta r} & \tau_{\theta\theta} & \tau_{\theta z} \\ \tau_{zr} & \tau_{z\theta} & \tau_{zz} \end{pmatrix} = \mu \begin{pmatrix} 2\dfrac{\partial u_r}{\partial r} & \dfrac{1}{r}\dfrac{\partial u_r}{\partial \theta} & 0 \\ \dfrac{1}{r}\dfrac{\partial u_r}{\partial \theta} & 2\dfrac{u_r}{r} & 0 \\ 0 & 0 & 0 \end{pmatrix}. \quad (3.4.23)$$

Substituting the stress components of the matrix (3.4.23) into equation (3.4.20) yields

$$\hat{r}\text{-component: } \rho\Big(\frac{\partial u_r}{\partial t} + u_r\frac{\partial u_r}{\partial r}\Big) = -\frac{\partial p}{\partial r} + \frac{1}{r}\frac{\partial}{\partial r}\left(2\mu r\frac{\partial u_r}{\partial r}\right) + \frac{1}{r}\frac{\partial}{\partial \theta}\left(\frac{\mu}{r}\frac{\partial u_r}{\partial \theta}\right) - 2\mu\frac{u_r}{r^2} + \rho F_r \quad (3.4.24)$$

and

$$\hat{\theta}\text{-component: } 0 = -\frac{1}{r}\frac{\partial p}{\partial \theta} + \frac{1}{r^2}\frac{\partial}{\partial r}\left(\mu r\frac{\partial u_r}{\partial \theta}\right) + \frac{1}{r}\frac{\partial}{\partial \theta}\left(2\mu\frac{u_r}{r}\right) + \rho F_\theta. \quad (3.4.25)$$

Expanding equation (3.4.24) yields

$$\begin{aligned}
\rho\left(\frac{\partial u_r}{\partial t}+u_r\frac{\partial u_r}{\partial r}\right) &= -\frac{\partial p}{\partial r}+\frac{1}{r}\frac{\partial}{\partial r}\left(2\mu r\frac{\partial u_r}{\partial r}\right)+\frac{1}{r}\frac{\partial}{\partial\theta}\left(\frac{\mu}{r}\frac{\partial u_r}{\partial\theta}\right)-2\mu\frac{u_r}{r^2}+\rho F_r \\
&= -\frac{\partial p}{\partial r}+\frac{2}{r}\left(\frac{\partial\mu}{\partial r}r\frac{\partial u_r}{\partial r}+\mu\frac{\partial u_r}{\partial r}+\mu r\frac{\partial^2 u_r}{\partial r^2}\right)+\frac{1}{r}\left(\frac{\partial\mu}{\partial\theta}\frac{1}{r}\frac{\partial u_r}{\partial\theta}+\frac{\mu}{r}\frac{\partial^2 u_r}{\partial\theta^2}\right) \\
&\quad -2\mu\frac{u_r}{r^2}+\rho F_r \\
&= -\frac{\partial p}{\partial r}+2\frac{\partial\mu}{\partial r}\frac{\partial u_r}{\partial r}+2\frac{\mu}{r}\frac{\partial u_r}{\partial r}+2\mu\frac{\partial^2 u_r}{\partial r^2}+\frac{1}{r^2}\frac{\partial\mu}{\partial\theta}\frac{\partial u_r}{\partial\theta}+\frac{\mu}{r^2}\frac{\partial^2 u_r}{\partial\theta^2} \\
&\quad -2\mu\frac{u_r}{r^2}+\rho F_r \\
\Rightarrow \rho\frac{\partial u_r}{\partial t} &= -\frac{\partial p}{\partial r}+2\frac{\partial\mu}{\partial r}\frac{\partial u_r}{\partial r}+\frac{1}{r^2}\frac{\partial\mu}{\partial\theta}\frac{\partial u_r}{\partial\theta}+\mu\left(\frac{1}{r^2}\frac{\partial^2 u_r}{\partial\theta^2}+2\frac{\partial^2 u_r}{\partial r^2}+\frac{2}{r}\frac{\partial u_r}{\partial r}-2\frac{u_r}{r^2}\right) \\
&\quad -\rho u_r\frac{\partial u_r}{\partial r}+\rho F_r
\end{aligned} \tag{3.4.26}$$

Expanding equation (3.4.25) yields

$$\begin{aligned}
0 &= -\frac{1}{r}\frac{\partial p}{\partial\theta}+\frac{1}{r^2}\frac{\partial}{\partial r}\left(\mu r\frac{\partial u_r}{\partial\theta}\right)+\frac{1}{r}\frac{\partial}{\partial\theta}\left(2\mu\frac{u_r}{r}\right)+\rho F_\theta \\
&= -\frac{1}{r}\frac{\partial p}{\partial\theta}+\frac{1}{r^2}\left(\frac{\partial\mu}{\partial r}r\frac{\partial u_r}{\partial\theta}+\mu\frac{\partial u_r}{\partial\theta}+\mu r\frac{\partial^2 u_r}{\partial r\partial\theta}\right)+\frac{2}{r}\left(\frac{\partial\mu}{\partial\theta}\frac{u_r}{r}+\frac{\mu}{r}\frac{\partial u_r}{\partial\theta}\right)+\rho F_\theta \\
&= -\frac{1}{r}\frac{\partial p}{\partial\theta}+\frac{1}{r}\frac{\partial\mu}{\partial r}\frac{\partial u_r}{\partial\theta}+\frac{\mu}{r^2}\frac{\partial u_r}{\partial\theta}+\frac{\mu}{r}\frac{\partial^2 u_r}{\partial r\partial\theta}+2\frac{u_r}{r^2}\frac{\partial\mu}{\partial\theta}+2\frac{\mu}{r^2}\frac{\partial u_r}{\partial\theta}+\rho F_\theta \\
&= -\frac{1}{r}\frac{\partial p}{\partial\theta}+\frac{1}{r}\frac{\partial\mu}{\partial r}\frac{\partial u_r}{\partial\theta}+3\frac{\mu}{r^2}\frac{\partial u_r}{\partial\theta}+\frac{\mu}{r}\frac{\partial^2 u_r}{\partial r\partial\theta}+2\frac{u_r}{r^2}\frac{\partial\mu}{\partial\theta}+\rho F_\theta \\
\Rightarrow\ -\frac{1}{r}\frac{\partial p}{\partial\theta} &+ \frac{1}{r}\frac{\partial\mu}{\partial r}\frac{\partial u_r}{\partial\theta}+\mu\left(\frac{3}{r^2}\frac{\partial u_r}{\partial\theta}+\frac{1}{r}\frac{\partial^2 u_r}{\partial r\partial\theta}\right)+2\frac{u_r}{r^2}\frac{\partial\mu}{\partial\theta}+\rho F_\theta=0.
\end{aligned} \tag{3.4.27}$$

Equations (3.4.26) and (3.4.27) represent the equation of motion in cylindrical coordinates for an unsteady two-dimensional laminar flow of an incompressible fluid whose motion is assumed to be symmetrical and purely radial.

Now, equations (3.4.4), (3.4.14), (3.4.26), and (3.4.27) are combined into one equation as follows:

Differentiating equation (3.4.4) partially with respect to r yields

$$\frac{\partial}{\partial r}\left(\frac{\partial u_r}{\partial r}+\frac{u_r}{r}\right)=\frac{\partial}{\partial r}(0)\quad\Rightarrow\frac{\partial^2 u_r}{\partial r^2}+\frac{1}{r}\frac{\partial u_r}{\partial r}-\frac{u_r}{r^2}=0. \tag{3.4.28}$$

Substituting equation (3.4.28) into equation (3.4.26) yields

$$\rho\frac{\partial u_r}{\partial t} = -\frac{\partial p}{\partial r} + 2\frac{\partial \mu}{\partial r}\frac{\partial u_r}{\partial r} + \frac{1}{r^2}\frac{\partial \mu}{\partial \theta}\frac{\partial u_r}{\partial \theta} + \frac{\mu}{r^2}\frac{\partial^2 u_r}{\partial \theta^2} - \rho u_r\frac{\partial u_r}{\partial r} + \rho F_r. \tag{3.4.29}$$

Differentiating equation (3.4.4) partially with respect to θ yields

$$\frac{\partial}{\partial \theta}\left(\frac{\partial u_r}{\partial r} + \frac{u_r}{r}\right) = \frac{\partial}{\partial \theta}(0) \quad \Rightarrow \frac{\partial^2 u_r}{\partial r \partial \theta} + \frac{1}{r}\frac{\partial u_r}{\partial \theta} = 0. \tag{3.4.30}$$

Substituting equation (3.4.30) into equation (3.4.27) yields

$$-\frac{1}{r}\frac{\partial p}{\partial \theta} + \frac{1}{r}\frac{\partial \mu}{\partial r}\frac{\partial u_r}{\partial \theta} + 2\frac{\mu}{r^2}\frac{\partial u_r}{\partial \theta} + 2\frac{u_r}{r^2}\frac{\partial \mu}{\partial \theta} + \rho F_\theta = 0. \tag{3.4.31}$$

Multiplying both sides of equation (3.4.31) by r yields

$$-\frac{\partial p}{\partial \theta} + \frac{\partial \mu}{\partial r}\frac{\partial u_r}{\partial \theta} + 2\frac{\mu}{r}\frac{\partial u_r}{\partial \theta} + 2\frac{u_r}{r}\frac{\partial \mu}{\partial \theta} + r\rho F_\theta = 0. \tag{3.4.32}$$

Substituting equation (3.4.14) into equation (3.4.29) yields

$$\frac{\partial u_r}{\partial t} = -\frac{1}{\rho}\frac{\partial p}{\partial r} + 2\frac{1}{\rho}\frac{\partial \mu}{\partial r}\frac{\partial u_r}{\partial r} + \frac{1}{\rho r^2}\frac{\partial \mu}{\partial \theta}\frac{\partial u_r}{\partial \theta} + \frac{\mu}{\rho r^2}\frac{\partial^2 u_r}{\partial \theta^2} - u_r\frac{\partial u_r}{\partial r} - \frac{\sigma B_0^2 u_r}{\rho} \tag{3.4.33}$$

Substituting equation (3.4.14) into equation (3.4.32) yields

$$-\frac{\partial p}{\partial \theta} + \frac{\partial \mu}{\partial r}\frac{\partial u_r}{\partial \theta} + 2\frac{\mu}{r}\frac{\partial u_r}{\partial \theta} + 2\frac{u_r}{r}\frac{\partial \mu}{\partial \theta} - \sigma B_0^2 r u_\theta = 0 \tag{3.4.34}$$

Since both the tangential and perpendicular velocities are negligible, equations (3.4.33) and (3.4.34) reduce to

$$\frac{\partial u_r}{\partial t} = -\frac{1}{\rho}\frac{\partial p}{\partial r} + 2\frac{1}{\rho}\frac{\partial \mu}{\partial r}\frac{\partial u_r}{\partial r} + \frac{1}{\rho r^2}\frac{\partial \mu}{\partial \theta}\frac{\partial u_r}{\partial \theta} + \frac{\mu}{\rho r^2}\frac{\partial^2 u_r}{\partial \theta^2} - u_r\frac{\partial u_r}{\partial r} - \frac{\sigma B_0^2 u_r}{\rho} \tag{3.4.35}$$

and

$$-\frac{\partial p}{\partial \theta}+\frac{\partial \mu}{\partial r}\frac{\partial u_r}{\partial \theta}+2\frac{\mu}{r}\frac{\partial u_r}{\partial \theta}+2\frac{u_r}{r}\frac{\partial \mu}{\partial \theta}=0, \tag{3.4.36}$$

respectively.

Differentiating equation (3.4.35) partially with respect to θ yields

$$\begin{aligned}
\frac{\partial}{\partial \theta}\left(\rho\frac{\partial u_r}{\partial t}\right) &= \frac{\partial}{\partial \theta}\left(-\frac{\partial p}{\partial r}+2\frac{\partial \mu}{\partial r}\frac{\partial u_r}{\partial r}+\frac{1}{r^2}\frac{\partial \mu}{\partial \theta}\frac{\partial u_r}{\partial \theta}+\frac{\mu}{r^2}\frac{\partial^2 u_r}{\partial \theta^2}-\rho u_r\frac{\partial u_r}{\partial r}-\sigma B_0^2 u_r\right)\\
\Rightarrow \rho\frac{\partial^2 u_r}{\partial \theta \partial t} &= -\frac{\partial^2 p}{\partial r \partial \theta}+2\frac{\partial^2 \mu}{\partial r \partial \theta}\frac{\partial u_r}{\partial r}+2\frac{\partial \mu}{\partial r}\frac{\partial^2 u_r}{\partial r \partial \theta}+\frac{1}{r^2}\frac{\partial^2 \mu}{\partial \theta^2}\frac{\partial u_r}{\partial \theta}+\frac{1}{r^2}\frac{\partial \mu}{\partial \theta}\frac{\partial^2 u_r}{\partial \theta^2}+\frac{1}{r^2}\frac{\partial \mu}{\partial \theta}\frac{\partial^2 u_r}{\partial \theta^2}\\
&\quad +\frac{\mu}{r^2}\frac{\partial^3 u_r}{\partial \theta^3}-\rho\frac{\partial u_r}{\partial \theta}\frac{\partial u_r}{\partial r}-\rho u_r\frac{\partial^2 u_r}{\partial r \partial \theta}-\sigma B_0^2\frac{\partial u_r}{\partial \theta}\\
\Rightarrow \frac{\partial^2 p}{\partial r \partial \theta} &= -\rho\frac{\partial^2 u_r}{\partial \theta \partial t}+2\frac{\partial^2 \mu}{\partial r \partial \theta}\frac{\partial u_r}{\partial r}+2\frac{\partial \mu}{\partial r}\frac{\partial^2 u_r}{\partial r \partial \theta}+\frac{1}{r^2}\frac{\partial^2 \mu}{\partial \theta^2}\frac{\partial u_r}{\partial \theta}+\frac{1}{r^2}\frac{\partial \mu}{\partial \theta}\frac{\partial^2 u_r}{\partial \theta^2}+\frac{1}{r^2}\frac{\partial \mu}{\partial \theta}\frac{\partial^2 u_r}{\partial \theta^2}\\
&\quad +\frac{\mu}{r^2}\frac{\partial^3 u_r}{\partial \theta^3}-\rho\frac{\partial u_r}{\partial \theta}\frac{\partial u_r}{\partial r}-\rho u_r\frac{\partial^2 u_r}{\partial r \partial \theta}-\sigma B_0^2\frac{\partial u_r}{\partial \theta}
\end{aligned} \tag{3.4.37}$$

Differentiating equation (3.4.36) partially with respect to r yields

$$\begin{aligned}
&\frac{\partial}{\partial r}\left(-\frac{\partial p}{\partial \theta}+\frac{\partial \mu}{\partial r}\frac{\partial u_r}{\partial \theta}+2\frac{\mu}{r}\frac{\partial u_r}{\partial \theta}+2\frac{u_r}{r}\frac{\partial \mu}{\partial \theta}-\sigma B_0^2 r u_\theta\right)=\frac{\partial}{\partial r}(0)\\
\Rightarrow\quad &-\frac{\partial^2 p}{\partial r \partial \theta}+\frac{\partial^2 \mu}{\partial r^2}\frac{\partial u_r}{\partial \theta}+\frac{\partial \mu}{\partial r}\frac{\partial^2 u_r}{\partial r \partial \theta}-2\frac{\mu}{r^2}\frac{\partial u_r}{\partial \theta}+\frac{2}{r}\frac{\partial \mu}{\partial r}\frac{\partial u_r}{\partial \theta}+2\frac{\mu}{r}\frac{\partial^2 u_r}{\partial r \partial \theta}-2\frac{u_r}{r^2}\frac{\partial \mu}{\partial \theta}+\frac{2}{r}\frac{\partial u_r}{\partial r}\frac{\partial \mu}{\partial \theta}\\
&+2\frac{u_r}{r}\frac{\partial^2 \mu}{\partial r \partial \theta}-\sigma B_0^2 r\frac{\partial u_\theta}{\partial r}-\sigma B_0^2 u_\theta=0\\
\Rightarrow \frac{\partial^2 p}{\partial r \partial \theta} &= \frac{\partial^2 \mu}{\partial r^2}\frac{\partial u_r}{\partial \theta}+\frac{\partial \mu}{\partial r}\frac{\partial^2 u_r}{\partial r \partial \theta}-2\frac{\mu}{r^2}\frac{\partial u_r}{\partial \theta}+\frac{2}{r}\frac{\partial \mu}{\partial r}\frac{\partial u_r}{\partial \theta}+2\frac{\mu}{r}\frac{\partial^2 u_r}{\partial r \partial \theta}-2\frac{u_r}{r^2}\frac{\partial \mu}{\partial \theta}+\frac{2}{r}\frac{\partial u_r}{\partial r}\frac{\partial \mu}{\partial \theta}\\
&\quad +2\frac{u_r}{r}\frac{\partial^2 \mu}{\partial r \partial \theta},\ \text{since}\ u_\theta=0
\end{aligned} \tag{3.4.38}$$

Eliminating the term involving p between equations (3.4.37) and (3.4.38) yields the following

nonlinear partial differential equation.

$$
\begin{aligned}
&-\rho\frac{\partial^2 u_r}{\partial\theta\partial t}+2\frac{\partial^2\mu}{\partial r\partial\theta}\frac{\partial u_r}{\partial r}+2\frac{\partial\mu}{\partial r}\frac{\partial^2 u_r}{\partial r\partial\theta}+\frac{1}{r^2}\frac{\partial^2\mu}{\partial\theta^2}\frac{\partial u_r}{\partial\theta}+\frac{1}{r^2}\frac{\partial\mu}{\partial\theta}\frac{\partial^2 u_r}{\partial\theta^2}+\frac{1}{r^2}\frac{\partial\mu}{\partial\theta}\frac{\partial^2 u_r}{\partial\theta^2}\\
&+\frac{\mu}{r^2}\frac{\partial^3 u_r}{\partial\theta^3}-\rho\frac{\partial u_r}{\partial\theta}\frac{\partial u_r}{\partial r}-\rho u_r\frac{\partial^2 u_r}{\partial r\partial\theta}-\sigma B_0^2\frac{\partial u_r}{\partial\theta}\\
&=\frac{\partial^2\mu}{\partial r^2}\frac{\partial u_r}{\partial\theta}+\frac{\partial\mu}{\partial r}\frac{\partial^2 u_r}{\partial r\partial\theta}-2\frac{\mu}{r^2}\frac{\partial u_r}{\partial\theta}+\frac{2}{r}\frac{\partial\mu}{\partial r}\frac{\partial u_r}{\partial\theta}+2\frac{\mu}{r}\frac{\partial^2 u_r}{\partial r\partial\theta}-2\frac{u_r}{r^2}\frac{\partial\mu}{\partial\theta}+\frac{2}{r}\frac{\partial u_r}{\partial r}\frac{\partial\mu}{\partial\theta}\\
&+2\frac{u_r}{r}\frac{\partial^2\mu}{\partial r\partial\theta}
\end{aligned}
$$

$$
\begin{aligned}
\Rightarrow\rho\frac{\partial^2 u_r}{\partial\theta\partial t} &= 2\frac{\partial^2\mu}{\partial r\partial\theta}\frac{\partial u_r}{\partial r}+2\frac{\partial\mu}{\partial r}\frac{\partial^2 u_r}{\partial r\partial\theta}+\frac{1}{r^2}\frac{\partial^2\mu}{\partial\theta^2}\frac{\partial u_r}{\partial\theta}+\frac{1}{r^2}\frac{\partial\mu}{\partial\theta}\frac{\partial^2 u_r}{\partial\theta^2}+\frac{1}{r^2}\frac{\partial\mu}{\partial\theta}\frac{\partial^2 u_r}{\partial\theta^2}\\
&+\frac{\mu}{r^2}\frac{\partial^3 u_r}{\partial\theta^3}-\rho\frac{\partial u_r}{\partial\theta}\frac{\partial u_r}{\partial r}-\rho u_r\frac{\partial^2 u_r}{\partial r\partial\theta}-\sigma B_0^2\frac{\partial u_r}{\partial\theta}\\
&-\frac{\partial^2\mu}{\partial r^2}\frac{\partial u_r}{\partial\theta}-\frac{\partial\mu}{\partial r}\frac{\partial^2 u_r}{\partial r\partial\theta}+2\frac{\mu}{r^2}\frac{\partial u_r}{\partial\theta}-\frac{2}{r}\frac{\partial\mu}{\partial r}\frac{\partial u_r}{\partial\theta}-2\frac{\mu}{r}\frac{\partial^2 u_r}{\partial r\partial\theta}+2\frac{u_r}{r^2}\frac{\partial\mu}{\partial\theta}-\frac{2}{r}\frac{\partial u_r}{\partial r}\frac{\partial\mu}{\partial\theta}\\
&-2\frac{u_r}{r}\frac{\partial^2\mu}{\partial r\partial\theta}
\end{aligned}
$$

$$
\begin{aligned}
\Rightarrow\frac{\partial^2 u_r}{\partial\theta\partial t} &= \frac{2}{\rho}\frac{\partial^2\mu}{\partial r\partial\theta}\frac{\partial u_r}{\partial r}+\frac{2}{\rho}\frac{\partial\mu}{\partial r}\frac{\partial^2 u_r}{\partial r\partial\theta}+\frac{1}{\rho r^2}\frac{\partial^2\mu}{\partial\theta^2}\frac{\partial u_r}{\partial\theta}+\frac{\partial\mu}{\partial\theta}\left(\frac{2}{\rho r^2}\frac{\partial^2 u_r}{\partial\theta^2}+2\frac{u_r}{\rho r^2}-\frac{2}{\rho r}\frac{\partial u_r}{\partial r}\right)\\
&+\frac{\mu}{\rho}\left(\frac{1}{r^2}\frac{\partial^3 u_r}{\partial\theta^3}+\frac{2}{r^2}\frac{\partial u_r}{\partial\theta}-\frac{2}{r}\frac{\partial^2 u_r}{\partial r\partial\theta}\right)-\frac{\partial u_r}{\partial\theta}\frac{\partial u_r}{\partial r}-u_r\frac{\partial^2 u_r}{\partial r\partial\theta}-\frac{1}{\rho}\frac{\partial^2\mu}{\partial r^2}\frac{\partial u_r}{\partial\theta}\\
&-\frac{1}{\rho}\frac{\partial\mu}{\partial r}\frac{\partial^2 u_r}{\partial r\partial\theta}-\frac{2}{\rho r}\frac{\partial\mu}{\partial r}\frac{\partial u_r}{\partial\theta}-2\frac{u_r}{\rho r}\frac{\partial^2\mu}{\partial r\partial\theta}-\frac{\sigma B_0^2}{\rho}\frac{\partial u_r}{\partial\theta}
\end{aligned}
\tag{3.4.39}
$$

Equation (3.4.39) is the reduced form of the equation of motion in cylindrical coordinates for an unsteady two-dimensional laminar flow of an incompressible fluid whose motion is symmetrical and purely radial.

3.4.4 Equation of energy

This is derived from the principle of conservation of energy which states that the amount of heat added to a system equals the change in internal energy and the work done. The general equation of energy, in vector notation, for an incompressible fluid is given by Salih (2011) as follows:

$$
\rho C_p\frac{DT}{Dt}=\rho\dot{q}_g+\vec{\nabla}\cdot(k\vec{\nabla}T)+\beta T\frac{D\rho}{Dt}+\Phi, \tag{3.4.40}
$$

where the viscous dissipation function Φ is given by

$$\Phi = \left(-\frac{2}{3}\mu\vec{\nabla}\cdot\vec{V}\,\bar{\bar{I}} + \mu\left[\vec{\nabla}\vec{V} + \left(\vec{\nabla}\vec{V}\right)^{\mathrm{T}}\right]\right) : \vec{\nabla}\vec{V}. \tag{3.4.41}$$

According to Salih (2011), equation (3.4.40), in cylindrical coordinates, is given by

$$\rho C_p\left(\frac{\partial T}{\partial t} + u_r\frac{\partial T}{\partial r} + \frac{u_\theta}{r}\frac{\partial T}{\partial \theta} + u_z\frac{\partial T}{\partial z}\right) = \rho\dot{q}_g + k\left[\frac{1}{r}\frac{\partial}{\partial r}\left(r\frac{\partial T}{\partial r}\right) + \frac{1}{r^2}\frac{\partial^2 T}{\partial \theta^2} + \frac{\partial^2 T}{\partial z^2}\right] + \Phi. \tag{3.4.42}$$

The viscous dissipation function Φ is given by the following expression:

$$\begin{aligned}\Phi &= 2\mu\left[\left(\frac{\partial u_r}{\partial r}\right)^2 + \left(\frac{1}{r}\frac{\partial u_\theta}{\partial \theta} + \frac{u_r}{r}\right)^2 + \left(\frac{\partial u_z}{\partial z}\right)^2\right] \\ &\quad +\mu\left[\left(\frac{1}{r}\frac{\partial u_r}{\partial \theta} + \frac{\partial u_\theta}{\partial r} - \frac{u_\theta}{r}\right)^2 + \left(\frac{\partial u_\theta}{\partial z} + \frac{1}{r}\frac{\partial u_z}{\partial \theta}\right)^2 + \left(\frac{\partial u_z}{\partial r} + \frac{\partial u_r}{\partial z}\right)^2\right].\end{aligned}$$

The dissipation function is non-negative since it only consists of squared terms. It represents a source of internal energy due to deformation work on the fluid particles. Since the flow is unbounded in the z-direction and both the tangential and perpendicular velocities are negligible, equation (3.4.42) reduces to

$$\rho C_p\left(\frac{\partial T}{\partial t} + u_r\frac{\partial T}{\partial r}\right) = k\left[\frac{1}{r}\frac{\partial}{\partial r}\left(r\frac{\partial T}{\partial r}\right) + \frac{1}{r^2}\frac{\partial^2 T}{\partial \theta^2}\right] + \Phi \tag{3.4.43}$$

and the viscous dissipation function becomes:

$$\Phi = 2\mu\left[\left(\frac{\partial u_r}{\partial r}\right)^2 + \left(\frac{u_r}{r}\right)^2\right] + \mu\left[\left(\frac{1}{r}\frac{\partial u_r}{\partial \theta}\right)^2\right]. \tag{3.4.44}$$

Dividing equation (3.4.43) by ρC_p and rearranging yields

$$\frac{\partial T}{\partial t} = \alpha\left[\frac{1}{r}\frac{\partial T}{\partial r} + \frac{\partial^2 T}{\partial r^2} + \frac{1}{r^2}\frac{\partial^2 T}{\partial \theta^2}\right] - u_r\frac{\partial T}{\partial r} + \frac{\mu}{\rho C_p}\left[2\left(\frac{\partial u_r}{\partial r}\right)^2 + 2\left(\frac{u_r}{r}\right)^2 + \left(\frac{1}{r}\frac{\partial u_r}{\partial \theta}\right)^2\right], \tag{3.4.45}$$

where the thermal diffusivity, α, is given by $\alpha = \dfrac{k}{\rho C_p}$.

Equation (3.4.45) represents the equation of energy in cylindrical coordinates for an unsteady two-

dimensional laminar flow of an incompressible fluid with a constant thermal conductivity.

3.5 Similarity transformation

In the present study, the resulting model is a system of two nonlinear partial differential equations −i.e., equations (3.4.39) and (3.4.45)− with the following boundary conditions which are formulated according to Mohyud-Din et al. (2016).

$$\begin{array}{ll} \text{At the centerline: } u_r = U_\infty, \dfrac{\partial u_r}{\partial \theta} = 0, \;\; T = T_\infty, \dfrac{\partial T}{\partial \theta} = 0 & \text{at } \theta = 0 \\ \text{On the walls: } \dfrac{\partial u_r}{\partial \theta} = -\gamma U(\theta), \;\; T = T_w & \text{at } \theta = \varpi \end{array}, \tag{3.5.1}$$

The boundary is said to be smooth if $\gamma = 0$ and perfectly rough if $\gamma \to \infty$. The interval $-|\varpi| < \theta < |\varpi|$ is the flow field domain. If it is require that the volumetric flow rate $Q \geq 0$, the flow is diverging from a source at $\theta = 0$ for $\varpi > 0$.

Since the resulting model is a system of nonlinear partial differential equations, it is convenient to simplify it by reducing the PDEs to ordinary differential equations since the solution of ODE is usually simpler. The technique of reducing PDEs to ODEs is known as similarity transformation. This technique is illustrated below.

From the continuity equation (3.4.4), define stream function $\Psi(r, \theta, t)$ such that equation (3.4.4) is satisfied. This is only possible if

$$\frac{\partial \Psi}{\partial \theta} = r u_r \text{ and } \frac{\partial \Psi}{\partial r} = 0. \tag{3.5.2}$$

From equation (3.5.2), it means that the stream function Ψ is independent of r. Thus, equation (3.5.2) can be written as

$$r u_r = f(\theta, t) \qquad \Rightarrow u_r = \frac{f(\theta, t)}{r} \tag{3.5.3}$$

From Rahman et al. (2016), potential function $u(r,t)$ is taken as follows:

$$u = \frac{\nu r^m}{\delta^{m+1}}. \tag{3.5.4}$$

According to Nagler (2017), u_r can be expressed as follows.

$$u_r = -\frac{QF(\theta)}{r}. \tag{3.5.5}$$

From equations (3.5.4) and (3.5.5), the following transformation is obtained.

$$u_r = -\frac{Q}{r}\frac{1}{\delta^{m+1}}F(\theta). \tag{3.5.6}$$

Comparing equations (3.5.3) and (3.5.6), it can be deduced that $f(\theta,t) = -Q\frac{1}{\delta^{m+1}}F(\theta)$. Therefore, equation (3.5.6) is the desired transformation for the fluid velocity.

From the power-law model (1.2.3), letting the velocity gradient $\frac{du}{dy}$ to be $g(\theta)$ yields the following transformation for the apparent viscosity:

$$\mu = \mu_0 g^{n-1}(\theta). \tag{3.5.7}$$

The velocity gradient is a function of θ only since it was found from the continuity equation (3.4.4) that the stream function Ψ is independent of r.

The similarity transformation for the temperature distribution is given by

$$\frac{\omega(\theta)}{\delta^{m+1}} = \frac{T - T_w}{T_\infty - T_w}. \tag{3.5.8}$$

Computing the respective partial derivatives yields

$$\begin{aligned}
\frac{\partial u_r}{\partial r} &= \frac{Q}{r^2}\frac{1}{\delta^{m+1}}F(\theta), \quad \frac{\partial u_r}{\partial \theta} = -\frac{Q}{r}\frac{1}{\delta^{m+1}}\frac{dF}{d\theta} \\
\frac{\partial^2 u_r}{\partial \theta \partial t} &= (m+1)\frac{Q}{r}\frac{1}{\delta^{m+2}}\frac{d\delta}{dt}\frac{dF}{d\theta} \\
\frac{\partial^2 u_r}{\partial r^2} &= -\frac{2Q}{r^3}\frac{1}{\delta^{m+1}}F(\theta), \quad \frac{\partial^2 u_r}{\partial r \partial \theta} = \frac{Q}{r^2}\frac{1}{\delta^{m+1}}\frac{dF}{d\theta}, \quad \frac{\partial^2 u_r}{\partial \theta^2} = -\frac{Q}{r}\frac{1}{\delta^{m+1}}\frac{d^2F}{d\theta^2} \\
\frac{\partial^3 u_r}{\partial \theta^3} &= -\frac{Q}{r}\frac{1}{\delta^{m+1}}\frac{d^3F}{d\theta^3}
\end{aligned}$$

$$\begin{aligned}
\frac{\partial \mu}{\partial r} &= 0, \quad \frac{\partial \mu}{\partial \theta} = \mu_0(n-1)g^{n-2}\frac{dg}{d\theta} \\
\frac{\partial^2 \mu}{\partial r^2} &= 0, \quad \frac{\partial^2 \mu}{\partial r \partial \theta} = 0, \quad \frac{\partial^2 \mu}{\partial \theta^2} = \mu_0(n-1)\left[(n-2)g^{n-3}\frac{dg}{d\theta}\frac{dg}{d\theta} + g^{n-2}\frac{d^2g}{d\theta^2}\right]
\end{aligned}$$

$$\begin{aligned}
\frac{\partial T}{\partial t} &= -(T_\infty - T_w)\frac{(m+1)}{\delta^{m+2}}\frac{d\delta}{dt}\omega, \quad \frac{\partial T}{\partial r} = 0, \quad \frac{\partial T}{\partial \theta} = (T_\infty - T_w)\frac{1}{\delta^{m+1}}\frac{d\omega}{d\theta} \\
\frac{\partial^2 T}{\partial r^2} &= 0, \quad \frac{\partial^2 T}{\partial \theta^2} = (T_\infty - T_w)\frac{1}{\delta^{m+1}}\frac{d^2\omega}{d\theta^2}
\end{aligned}$$

Substituting the above differentials into equation (3.4.39) yields

$$\begin{aligned}
(m+1)\frac{Q}{r}\frac{1}{\delta^{m+2}}\frac{d\delta}{dt}\frac{dF}{d\theta} &= \frac{1}{\rho r^2}\mu_0(n-1)\left[(n-2)g^{n-3}\frac{dg}{d\theta}\frac{dg}{d\theta} + g^{n-2}\frac{d^2g}{d\theta^2}\right]\left[-\frac{Q}{r}\frac{1}{\delta^{m+1}}\frac{dF}{d\theta}\right] \\
&\quad +\mu_0(n-1)g^{n-2}\frac{dg}{d\theta}\left(-\frac{2Q}{\rho r^3}\frac{1}{\delta^{m+1}}\frac{d^2F}{d\theta^2} - \frac{2Q}{\rho r^3}\frac{1}{\delta^{m+1}}F(\theta) - \frac{2Q}{\rho r^3}\frac{1}{\delta^{m+1}}F(\theta)\right) \\
&\quad +\mu_0 g^{n-1}(\theta)\left(-\frac{Q}{\rho r^3}\frac{1}{\delta^{m+1}}\frac{d^3F}{d\theta^3} - \frac{2Q}{\rho r^3}\frac{1}{\delta^{m+1}}\frac{dF}{d\theta} - \frac{2Q}{\rho r^3}\frac{1}{\delta^{m+1}}\frac{dF}{d\theta}\right) \\
&\quad +\frac{Q^2}{r^3}\frac{1}{\delta^{2m+2}}F(\theta)\frac{dF}{d\theta} + \frac{Q^2}{r^3}\frac{1}{\delta^{2m+2}}F(\theta)\frac{dF}{d\theta} + \frac{\sigma B_0^2}{\rho}\frac{Q}{r}\frac{1}{\delta^{m+1}}\frac{dF}{d\theta}. \qquad (3.5.9)
\end{aligned}$$

Multiplying equation (3.5.9) by δ^{m+1} and then simplifying yields.

$$\begin{aligned}
(m+1)\frac{Q}{r}\frac{1}{\delta}\frac{d\delta}{dt}F' &= -\frac{Q}{\rho r^3}\mu_0(n-1)\left[(n-2)g^{n-3}g'^2 + g^{n-2}g''\right]F' \\
&\quad -\frac{Q}{\rho r^3}\mu_0(n-1)g^{n-2}g'\left[2F'' + 4F\right] \\
&\quad -\frac{Q}{\rho r^3}\mu_0 g^{n-1}\left[F''' + 4F'\right] + \frac{2Q^2}{r^3}\frac{1}{\delta^{m+1}}FF' + \frac{\sigma B_0^2}{\rho}\frac{Q}{r}F'. \qquad (3.5.10)
\end{aligned}$$

Multiplying both sides of equation (3.5.10) by $\rho r^3/\mu_0 Q$ and rearranging yields

$$(n-1)\left[(n-2)g^{n-3}g'^2+g^{n-2}g''\right]F'+(n-1)g^{n-2}g'\left[2F''+4F\right]$$
$$+g^{n-1}\left[F'''+4F'\right]-2\frac{Q\rho}{\mu_0}\frac{1}{\delta^{m+1}}FF'-\frac{\sigma B_0^2 r^2}{\mu_0}F'+(m+1)\frac{\rho r^2}{\mu_0}\frac{1}{\delta}\frac{d\delta}{dt}F'=0. \quad (3.5.11)$$

In order to make the governing equations locally similar, define the unsteadiness parameter λ according to Rahman et al. (2016) as follows:

$$\lambda=\frac{\rho\delta^m}{\mu_0 r^{m-1}}\frac{d\delta}{dt}. \quad (3.5.12)$$

This parameter will account for the time factor. equation (3.5.12) is sometimes called the locally similar equation. Thus, equation (3.5.11) can be factorized in terms of the unsteadiness parameter as follows:

$$(n-1)\left[(n-2)g^{n-3}g'^2+g^{n-2}g''\right]F'+(n-1)g^{n-2}g'\left[2F''+4F\right]$$
$$+g^{n-1}\left[F'''+4F'\right]-2\frac{Q\rho}{\mu_0}\frac{1}{\delta^{m+1}}FF'-\frac{\sigma B_0^2 r^2}{\mu_0}F'$$
$$+(m+1)\frac{r^{m+1}}{\delta^{m+1}}\left(\frac{\rho\delta^m}{\mu_0 r^{m-1}}\frac{d\delta}{dt}\right)F'=0. \quad (3.5.13)$$

Since the factors $\dfrac{Q\rho}{\mu_0}$ denotes the Reynolds number, $B_0 r\left(\dfrac{\sigma}{\mu_0}\right)^{\frac{1}{2}}$ denotes the Hartmann number, and $\dfrac{\rho\delta^m}{\mu_0 r^{m-1}}\dfrac{d\delta}{dt}$ represents the unsteadiness parameter, equation (3.5.13) becomes:

$$(n-1)\left[(n-2)g^{n-3}g'^2+g^{n-2}g''\right]F'+(n-1)g^{n-2}g'\left[2F''+4F\right]$$
$$+g^{n-1}\left[F'''+4F'\right]-2Re\frac{1}{\delta^{m+1}}FF'-Ha^2F'+(m+1)\frac{r^{m+1}}{\delta^{m+1}}\lambda F'=0. \quad (3.5.14)$$

Similarly, substituting the above differentials into equation (3.4.45) yields

$$\begin{aligned} -(T_\infty - T_w)\frac{(m+1)}{\delta^{m+2}}\frac{d\delta}{dt}\omega &= \alpha\left[\frac{1}{r^2}(T_\infty - T_w)\frac{1}{\delta^{m+1}}\frac{d^2\omega}{d\theta^2}\right] \\ &+\frac{\mu_0}{\rho C_p}g^{n-1}(\theta)\left[2\left(\frac{Q}{r^2}\frac{1}{\delta^{m+1}}F(\theta)\right)^2 + 2\left(-\frac{Q}{r^2}\frac{1}{\delta^{m+1}}F(\theta)\right)^2\right] \\ &+\frac{\mu_0}{\rho C_p}g^{n-1}(\theta)\left[\left(-\frac{1}{r}\frac{Q}{r}\frac{1}{\delta^{m+1}}\frac{dF}{d\theta}\right)^2\right]. \end{aligned} \tag{3.5.15}$$

Simplifying yields the following equation:

$$-(T_\infty - T_w)\frac{(m+1)}{\delta^{m+2}}\frac{d\delta}{dt}\omega = (T_\infty - T_w)\frac{\alpha}{r^2}\frac{1}{\delta^{m+1}}\omega'' + \frac{\mu_0 Q^2/r^4}{\rho C_p}\frac{1}{\delta^{2m+2}}g^{n-1}\left[4F^2 + F'^2\right] \tag{3.5.16}$$

Multiplying both sides of equation (3.5.16) by $\frac{\rho r^2\delta^{m+1}}{\mu_0(T_\infty - T_w)}$ and rearranging yields

$$\frac{\alpha\rho}{\mu_0}\omega'' + (m+1)\frac{\rho r^2}{\mu_0\delta}\frac{d\delta}{dt}\omega + \frac{Q^2/r^2}{C_p(T_\infty - T_w)}\frac{1}{\delta^{m+1}}g^{n-1}\left[4F^2 + F'^2\right] = 0. \tag{3.5.17}$$

Equation (3.5.17) can be factorized in terms of the unsteadiness parameter as follows:

$$\frac{\alpha\rho}{\mu_0}\omega'' + (m+1)\frac{r^{m+1}}{\delta^{m+1}}\left(\frac{\rho\delta^m}{\mu_0 r^{m-1}}\frac{d\delta}{dt}\right)\omega + \frac{Q^2/r^2}{C_p(T_\infty - T_w)}\frac{1}{\delta^{m+1}}g^{n-1}\left[4F^2 + F'^2\right] = 0. \tag{3.5.18}$$

Since the factors $\frac{\mu_0}{\rho\alpha}$ denotes the Prandtl number, $\frac{Q^2/r^2}{C_p(T_\infty - T_w)}$ denotes the Eckert number, and $\frac{\rho\delta^m}{\mu_0 r^{m-1}}\frac{d\delta}{dt}$ denotes the unsteadiness parameter, equation (3.5.18) becomes

$$\frac{1}{Pr}\omega'' + (m+1)\frac{r^{m+1}}{\delta^{m+1}}\lambda\omega + \frac{Ec}{\delta^{m+1}}g^{n-1}\left[4F^2 + F'^2\right] = 0. \tag{3.5.19}$$

3.5.1 Final set of the governing equations in dimensionless form

The implementation of similarity transformation technique reduces the momentum equation (3.4.39) to

$$\begin{aligned}&(n-1)\left[(n-2)g^{n-3}g'^2+g^{n-2}g''\right]F'+(n-1)g^{n-2}g'\left[2F''+4F\right]\\&+g^{n-1}\left[F'''+4F'\right]-2Re\frac{1}{\delta^{m+1}}FF'-Ha^2F'+(m+1)\frac{r^{m+1}}{\delta^{m+1}}\lambda F'=0,\end{aligned}\tag{3.5.20}$$

and the energy equation (3.4.45) to

$$\frac{1}{Pr}\omega''+(m+1)\frac{r^{m+1}}{\delta^{m+1}}\lambda\omega+\frac{Ec}{\delta^{m+1}}g^{n-1}\left[4F^2+F'^2\right]=0.\tag{3.5.21}$$

In order to simplify the solution(s) of the model, the following expression for the velocity gradient g is considered:

$$g=\theta^c,\ \ c\geq 2,\tag{3.5.22}$$

where c is an arbitrary constant. Differentiating equation (3.5.22) with respect to θ yields

$$g' = c\theta^{c-1}\tag{3.5.23}$$

$$g'' = c(c-1)\theta^{c-2}\tag{3.5.24}$$

Substituting equations (3.5.22), (3.5.23), and (3.5.24) into equation (3.5.20) yields

$$\begin{aligned}&(n-1)\left[(n-2)\theta^{c(n-3)}c^2\theta^{2c-2}+\theta^{c(n-2)}c(c-1)\theta^{c-2}\right]F'\\&+(n-1)\theta^{c(n-2)}c\theta^{c-1}\left[2F''+4F\right]+\theta^{c(n-1)}\left[F'''+4F'\right]\\&-2Re\frac{1}{\delta^{m+1}}FF'-Ha^2F'+(m+1)\frac{r^{m+1}}{\delta^{m+1}}\lambda F'=0.\end{aligned}\tag{3.5.25}$$

Simplifying equation (3.5.25) yields

$$c(n-1)\theta^{c(n-1)-2}\left[c(n-1)-1\right]F' + c(n-1)\theta^{c(n-1)-1}\left[2F'' + 4F\right]$$
$$+\theta^{c(n-1)}\left[F''' + 4F'\right] - 2Re\frac{1}{\delta^{m+1}}FF' - Ha^2F' + (m+1)\frac{r^{m+1}}{\delta^{m+1}}\lambda F' = 0. \quad (3.5.26)$$

Similarly, substituting equation (3.5.22) into equation (3.5.21) yields

$$\frac{1}{Pr}\omega'' + (m+1)\frac{r^{m+1}}{\delta^{m+1}}\lambda\omega + \frac{Ec}{\delta^{m+1}}\theta^{c(n-1)}\left[4F^2 + F'^2\right] = 0. \quad (3.5.27)$$

Thus, equations (3.5.26) and (3.5.27) are the final set of the locally similar governing equations in dimensionless form. These equations are subjected to the following boundary conditions:

3.5.2 Boundary conditions

The above similarity transformations are applied to the boundary conditions (3.5.1) as follows:

From equation (3.5.6) it is deduced that

$$u_r = -\frac{Q}{r}\frac{1}{\delta^{m+1}}F(\theta). \quad (3.5.28)$$

Differentiating equation (3.5.28) partially with respect to θ yields

$$\frac{\partial u_r}{\partial\theta} = -\frac{Q}{r}\frac{1}{\delta^{m+1}}F'(\theta) = -\gamma\frac{Q}{r}\frac{1}{\delta^{m+1}}F(\theta). \quad (3.5.29)$$

Therefore,

$$F'(\theta) = -\gamma F(\theta) \text{ at } \theta = \varpi. \quad (3.5.30)$$

From equation (3.5.30), it is deduced that

$$F'(0) = -\gamma F(0) = 0 \text{ at } \theta = 0. \tag{3.5.31}$$

Due to the flow symmetry assumption, the condition (3.5.30) is simply written as

$$F'(\varpi) = -\gamma F(\varpi). \tag{3.5.32}$$

From equation (3.5.8), putting $T = T_w$ yields

$$\frac{\omega(\theta)}{\delta^{m+1}} = \frac{T_w - T_w}{T_\infty - T_w} = 0 \quad \Rightarrow \omega(\varpi) = 0. \tag{3.5.33}$$

Also from equation (3.5.8), putting $T = T_\infty$ yields

$$\frac{\omega(\theta)}{\delta^{m+1}} = \frac{T_\infty - T_w}{T_\infty - T_w} = 1 \quad \Rightarrow \omega(0) = \delta^{m+1}. \tag{3.5.34}$$

Thus, the implementation of similarity transformation technique reduces the boundary conditions (3.5.1) to the dimensionless form given by

$$\begin{aligned} &\text{At the centerline: } F(0) = 1,\ F'(0) = 0,\ \omega(0) = \delta^{m+1} && \text{at } \theta = 0 \\ &\text{On the walls: } F'(\varpi) = -\gamma F(\varpi),\ \omega(\varpi) = 0 && \text{at } \theta = \varpi \end{aligned} \tag{3.5.35}$$

3.6 Flow parameters and their significance

The similarity transformation technique gave rise to the dimensionless numbers discussed below.

3.6.1 Reynolds number

The Reynolds number (Re) is a dimensionless number defined as the ratio of inertial force to viscous force (Batchelor, 2000). It is expressed as

$$Re = \frac{\text{inertial force}}{\text{viscous force}} = \frac{Q\rho}{\mu_0}.$$

When Re of the system is very small (i.e., $Re << 1$), the viscous force is predominant and the flow is said to be laminar (i.e., sheet-like flow). On the other hand, if Re is very large (i.e., $Re >> 1$), the inertial force is predominant which produces chaotic eddies, vortices, and other flow instabilities. Thus, turbulent flow occurs at high Reynolds numbers. If, for any flow, this number is less than one then the inertia force is negligible. Otherwise, viscous force can be ignored and so the fluid can be taken as inviscid.

3.6.2 Hartmann number

The Hartmann number (Ha) is a dimensionless number defined as the square root of the ratio of the electromagnetic force to viscous force (Batchelor, 2000). It can be expressed as

$$Ha = \Big(\frac{\text{electromagnetic force}}{\text{viscous force}}\Big)^{\frac{1}{2}} = B_0 r\Big(\frac{\sigma}{\mu_0}\Big)^{\frac{1}{2}}.$$

3.6.3 Prandtl number

The Prandtl number (Pr) is a dimensionless number defined as the ratio of momentum diffusivity (kinematic viscosity) to thermal diffusivity (Batchelor, 2000). It can be expressed as

$$Pr = \frac{\text{momentum diffusivity}}{\text{thermal diffusivity}} = \frac{\mu_0}{\rho\alpha}.$$

The Prandtl number is often used in convective heat transfer. Small values of the Prandtl number, $Pr << 1$, means that the thermal diffusivity dominates. Whereas with large values, $Pr >> 1$, the

momentum diffusivity dominates.

3.6.4 Eckert number

The Eckert number (Ec) is a dimensionless number defined as the ratio of the advective mass transfer to the heat dissipation potential (Batchelor, 2000). It is used to characterize heat dissipation in high-speed flows for which viscous dissipation is significant. It can be expressed as

$$Ec = \frac{\text{heat dissipation potential}}{\text{advective mass transfer}} = \frac{Q^2/r^2}{C_p(T_\infty - T_w)},$$

where $T_\infty - T_w$ is the temperature gradient. For small Eckert number ($Ec << 1$) the terms in the energy equation describing the effects of pressure changes, viscous dissipation, and body forces on the energy balance can be neglected and the equation reduces to a balance between conduction and convection.

The Eckert number, when multiplied by the Prandtl number, is also a key parameter in determining the viscous dissipation of energy in a low-speed flow. The parameter $Ec \cdot Pr$ (sometimes called the Brinkman number) is essentially the ratio of the kinetic energy dissipated in the flow to the thermal energy conducted into or away from the fluid. When $(Ec \cdot Pr) << 1$, the energy dissipation can be neglected relative to heat conduction in the fluid. For large $Ec \cdot Pr$, the energy dissipated is an important parameter in the heat transfer process and the kinetic energy can play a significant role in determining the temperature distribution in the flow and the overall heat transfer.

The next chapter presents the numerical method used to solve the model equations and the corresponding simulation.

Chapter 4

Method of Solution

4.1 Introduction

In most cases, differential equations governing scientific problems such as Jeffery-Hamel flow are inherently nonlinear. Due to the nonlinearity of the resulting partial differential equations, an analytical solution is not possible. These nonlinear equations are solved using approximation methods (i.e., numerical techniques or semi-analytical methods) in order to obtain non-analytical solutions. According to Domairry et al. (2009), the semi-analytical methods include homotopy perturbation method (HPM), homotopy analysis method (HAM) and differential transform method (DTM). However, most of these semi-analytical techniques are either very difficult to employ and require a lot of computation or the level of accuracy has to be compromised; which not only affects the results badly but (in some cases) they become completely unreliable (Khan et al., 2013). Therefore, different numerical techniques for boundary value problems (BVP) are employed in solving these nonlinear differential equations.

There are three important properties of a numerical technique that must be considered in choosing the best method for solving a particular problem. They include convergence, consistency, and stability. A very powerful and quite a general method for solving most BVPs is the collocation method. Collocation method has been tested by Hale (2006) for convergence, consistency, and stability. This study uses collocation method to solve the resulting model equations since it is a successful method for solving two-point BVPs. This method is discussed below.

4.2 Collocation Method

This is a highly stable numerical technique that estimates the solution of a BVP using a polynomial and makes use of solvers that take low computational memory. Hence, it is more advantageous to use in boundary value problems than other numerical techniques. The advantage of collocation method is that it provides a continuous approximation to the solution whereas many other numerical methods

produce only a table of values of the approximate solution at discrete points.

4.2.1 Overview of Collocation Method

Suppose there is a differential operator D acting on a function $y(\theta)$ to produce another function $p(\theta)$ (Petroudi et al., 2014):

$$D[y(\theta)] = p(\theta), \tag{4.2.1}$$

where $y(\theta)$ is the exact solution of the BVP. The solution $y(\theta)$ is approximated over $[\theta_0, \theta_N]$ by a piecewise polynomial $Y(\theta)$ over each subinterval $[\theta_i, \theta_{i+1}]$. The function $Y(\theta)$, which is expressed as a linear combination of basis functions chosen from a linearly independent set, will satisfy the ODE at selected collocation points within each interval. The approximate solution is expressed as follows:

$$y \approx Y = \psi_0(\theta) + \sum_{\kappa=1}^{N} c_\kappa \psi_\kappa(\theta), \tag{4.2.2}$$

where the functions $\psi_\kappa(\theta)$ satisfy the given boundary conditions. Now, substituting equation (4.2.2) into equation (4.2.1) yields $D[Y(\theta)] \approx p(\theta)$. Hence, a residual exists and is defined by

$$R(\theta) = D[Y(\theta)] - p(\theta) \neq 0. \tag{4.2.3}$$

The residual tells us how much the approximate solution does not satisfy the governing equation. It is not the same as error.

Since it is difficult to make the residual identically equal to zero, it is minimized by setting the weighted integral of the residual equal to zero. That is

$$\int_{\theta_0}^{\theta_N} W_\kappa(\theta) R(\theta) d\theta = 0, \ \kappa = 1, 2, \cdots, N \ , \tag{4.2.4}$$

where the number of weight functions W_κ are exactly equal the number of unknown constants c_κ in $Y(\theta)$. The result is a set of N algebraic equations for the unknown constants c_κ.. For collocation method, the weighting functions are taken from the family of Dirac δ functions in the domain. That

is, $W_\kappa = \delta(\theta - \theta_\kappa)$. The Dirac δ function has the property that

$$\delta(\theta - \theta_\kappa) = \begin{cases} 1 & \text{if } \theta = \theta_\kappa \\ 0 & \text{otherwise.} \end{cases} \tag{4.2.5}$$

Thus, the task is to solve the following system of algebraic equations

$$R(\theta_\kappa, \{c_\kappa\}) = 0 \text{ for } \kappa = 1, 2, \cdots, N \tag{4.2.6}$$

and determine the interior collocation solutions $c_1, c_2, \cdots, c_N$.

The locally similar and nonlinear ordinary differential equations (3.5.12), (3.5.26) and (3.5.27) together with the boundary conditions (3.5.35) are solved numerically by collocation method. The model equations are first reduced to a system of first-order ODEs together with the corresponding boundary conditions. The reduction of order technique is illustrated below.

4.3 Reduction of order

It is convenient when solving an ODE system numerically to describe the problem in terms of a system of first-order equations. To reduce the model equations (3.5.26) and (3.5.27) to a system of first order ordinary differential equations together with the corresponding boundary conditions (3.5.35), let

$$y_1 = F, y_2 = F', y_3 = F'', y_4 = \omega, \text{ and } y_5 = \omega'$$

Therefore,

$$\begin{aligned}
y_1' &= y_2 \\
y_2' &= y_3 \\
y_3' &= \Big[-c(n-1)\theta^{c(n-1)-2} \left[c(n-1)-1\right] y_2 - c(n-1)\theta^{c(n-1)-1} \left[2y_3 + 4y_1\right] \\
&\quad -(m+1)\frac{r^{m+1}}{\delta^{m+1}}\lambda y_2 + 2Re\frac{1}{\delta^{m+1}} y_1 y_2 + Ha^2 y_2 \Big] / \theta^{c(n-1)} - 4y_2 \\
y_4' &= y_5 \\
y_5' &= -Pr\left[(m+1)\frac{r^{m+1}}{\delta^{m+1}}\lambda y_4 + \frac{Ec}{\delta^{m+1}}\theta^{c(n-1)}\left[4y_1^2 + y_2^2\right]\right]
\end{aligned} \tag{4.3.1}$$

The corresponding boundary conditions become:

$$\begin{aligned} &\text{At the centerline: } y_1(0) - 1 = 0, \;\; y_2(0) = 0, \;\; y_4(0) - \delta^{m+1} = 0 \quad \text{at } \theta = 0 \\ &\text{On the walls: } y_2(\varpi) + \gamma y_1(\varpi) = 0, \;\; y_4(\varpi) = 0 \qquad\qquad\qquad\quad \text{at } \theta = \varpi \end{aligned} \tag{4.3.2}$$

Equations (4.3.1) and (4.3.2) will be helpful during simulation of the model equations. Thus, adopting the collocation technique, a computer program has been set up for the solution of the governing coupled nonlinear ordinary differential equations of the current problem with the aid of the inbuilt MATLAB function known as bvp4c. The bvp4c algorithm is the most convenient since it is able to give optimal solutions that are accurate. This algorithm is discussed below.

4.4 Bvp4c framework

Kierzenka and Shampine (2001) developed the software bvp4c to implement collocation method for the solution of two-point BVPs of the form

$$y' = f(\theta, y, p), \; a \leq \theta \leq b$$

subject to general nonlinear, two-point boundary conditions

$$g(y(a), y(b), p) = 0$$

Here p is a vector of unknown parameters.

The first step in solving a problem is defining it in a way the software can understand. Thus the bvp4c algorithm requires that the model equations (3.5.26) and (3.5.27) be reduced to a system of first-order ordinary differential equations as described in section 4.3. Similarly, the user then rewrites the boundary conditions to correspond to this form of the problem. The bvp4c framework uses a number of subfunctions which make it easier for the user to enter the ODE function, initial data and parameters for a given problem.

```
% first-order system of ODEs for the model equations.
function dydx = odeFunction(theta,y)
  .
  .
  .
end

% Boundary conditions for the model equations.
function res = bcFunction(ya,yb)
  .
  .
  .
end
```

The next step is to create an initial guess for the form of the solution using a specific MATLAB subroutine called bvpinit. The user passes a vector x and an initial guess on this mesh in the form

```
bvpinit(x, Yinit),
```

which is then converted into a structure useable by bvp4c. The user would define

```
options = bvpset('stats','on','reltol',1e-4,'abstol',1e-4);
solinit = bvpinit(linspace(0,1,5),[1 0],3.14);
```

and call the bvp4c routine with

```
sol = bvp4c(@odeFunction,@bcFunction,solinit,options);
```

Whereas the bvpinit function defines the initial properties of the problem, the bvpset function specifies which options bvp4c should be use in solving it. The above essentially ends the user input in solving the BVP system and the rest is left to bvp4c. The bvp4c framework has been expounded in Hale (2006). Appendix A.2 shows the MATLAB code used to simulate equations (3.5.26) and (3.5.27) with the help of bvp4c framework. The graphical solutions obtained are discussed in Chapter 5.

4.5 Skin-friction coefficient and rate of heat transfer

The local skin-friction coefficient and wall heat transfer rate can be obtained from the following expressions according to Rahman et al. (2016).

Skin-friction coefficient:

$$C_f = \frac{2}{\sqrt{Re(2-\epsilon)}} F'(0)$$

Nusselt number:

$$N_u = -\sqrt{\frac{Re}{(2-\epsilon)}} \omega'(0)$$

Appendix A.2 shows the MATLAB code used to compute the skin-friction coefficient and rate of heat transfer. The results obtained are shown in Table 5.1.

4.6 Validation

A comparison of the results obtained from this study with Pavithra and Gireesha (2014) is tabulated in Table 4.1. From the table, it is clear that there is a close agreement between the results which verifies the accuracy of the method used in the present study.

Table 4.1: Comparison of the results for the dimensionless temperature gradient $-\omega'(0)$ by varying the Pr with $Re = Ha = Ec = 0$.

Pr	Pavithra and Gireesha (2014)	Present study
0.72	0.76762	0.76782
1.0	0.95474	0.95479
2.0	1.47144	1.47148
3.0	1.86904	1.86909
5.0	2.50012	2.50016

The next chapter presents the results of the present study and their significance to real life in terms of application.

Chapter 5

Results and Discussion

5.1 Overview

This chapter presents the velocity profiles, temperature profiles, skin-friction coefficient, and rate of heat transfer for $Re \in [3, 25]$, $Ha \in [0.5, 5]$, $Pr \in [0.5, 5]$, $Ec \in [2, 10]$, and $\lambda \in [1.5, 15]$. The effects of varying the flow parameters on the velocity profiles, temperature profiles, skin-friction coefficient, and rate of heat transfer have been determined using simulation. The other parameters such as wedge angle ϖ, flow behavior index n, friction coefficient factor γ, time-dependent length scale δ, and the constants c and m are kept constant throughout. The results are presented in form of graphs and tables.

5.2 Effects of Varying Reynolds number on Velocity and Temperature Profiles

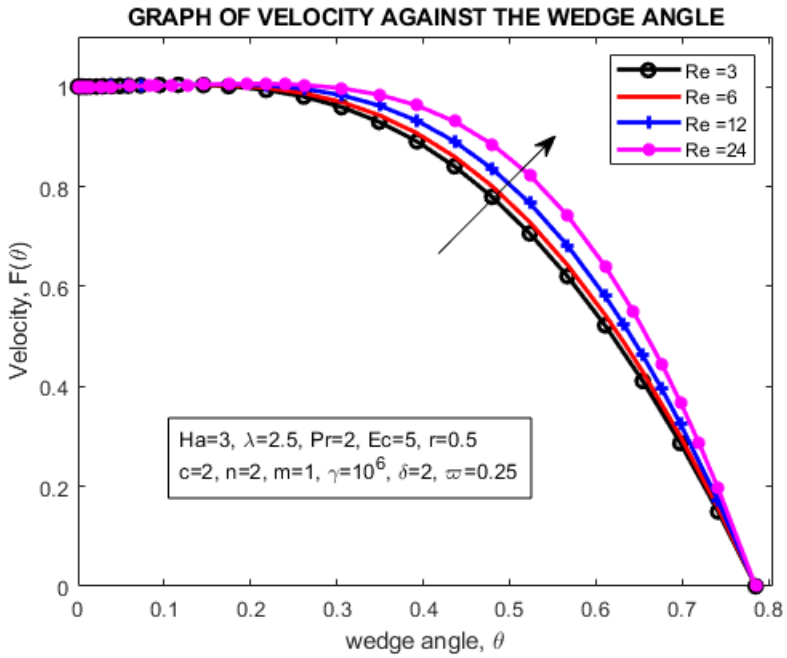

Figure 5.1: Effects of Re on velocity profiles.

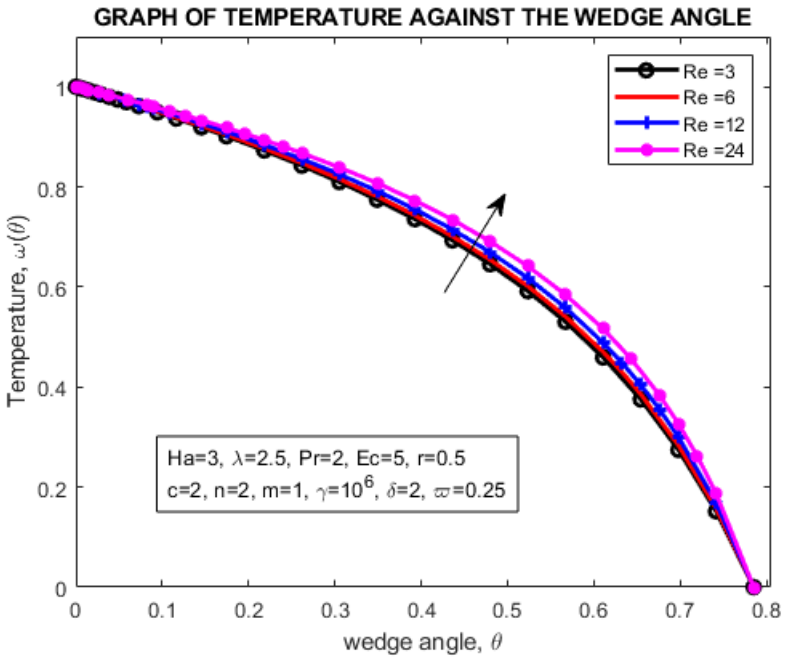

Figure 5.2: Effects of Re on temperature profiles.

It is noted from Figure 5.1 that an increase in Reynolds number increases the fluid velocity. This is because a small Reynolds number implies that the viscous force is predominant and as a result, there will be a retardation of the flow due to the formation and extension of the boundary layer into the flow region. Conversely, a large Reynolds number implies that the viscous force is less predominant and as a result, there will be less retardation of the flow since the boundary layer formed does not really extend into the flow region. Thus high Reynolds number indicates turbulent flow and erratic velocity profiles.

It is noted from Figure 5.2 that an increase in Reynolds number increases the fluid temperature. This is because an increase in the Reynolds number means that the viscous force becomes less predominant and hence the fluid viscosity decreases. Since viscosity and temperature are inversely proportional in liquids, a decrease in viscosity implies an increase in the fluid temperature. Thus the heat transfer reduction range is enlarged.

5.3 Effects of Varying Hartman number on Velocity and Temperature Profiles

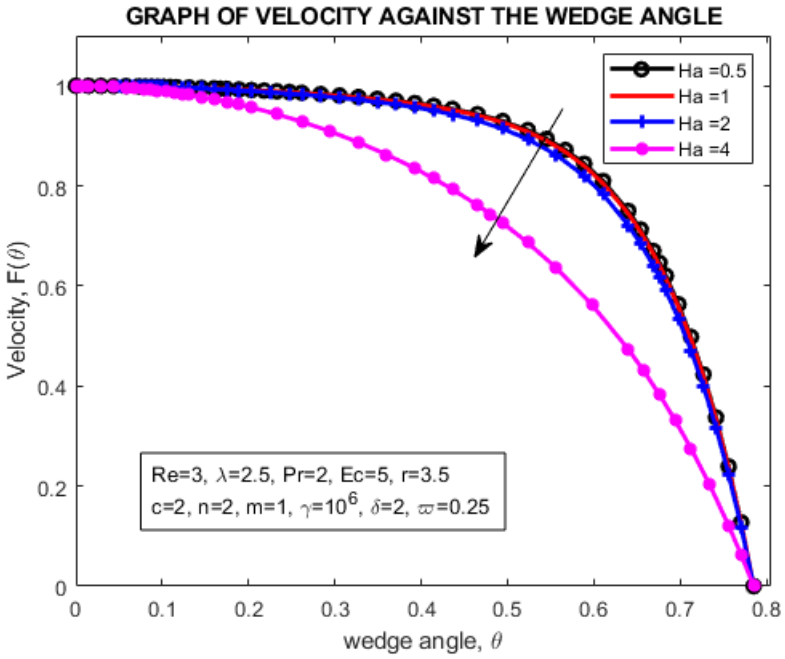

Figure 5.3: Effects of Ha on velocity profiles.

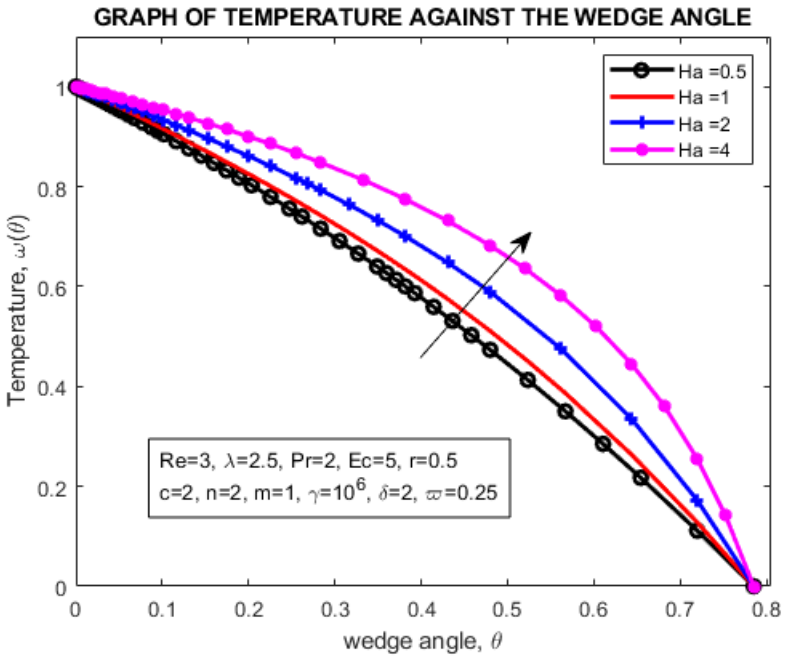

Figure 5.4: Effects of Ha on temperature profiles.

It is noted from Figure 5.3 that an increase in Hartmann number increases the fluid velocity. This is because the application of a magnetic field moving with the freestream has the tendency to induce an electromagnetic force known as the Lorentz force which increases the hydrodynamic boundary layer thickness. So, increasing the value of the Hartmann increases the Lorentz force which suppresses the transport phenomenon. The Hartmann number gives a measure of the relative importance of drag forces resulting from magnetic induction and viscous forces in Hartmann flow, and determines the velocity profile for such flow.

It is noted from Figure 5.4 that an increase in Hartmann number increases the fluid temperature. This is because application of magnetic field to an electrically conducting fluid gives rise to a magnetic force called the Lorentz force. Increase in Hartmann number increases the Lorentz force which then raises the temperature of the fluid. At high operating temperature, high Hartmann number is quite significant in the heat transfer phenomenon.

5.4 Effects of Varying Prandtl number on Velocity and Temperature Profiles

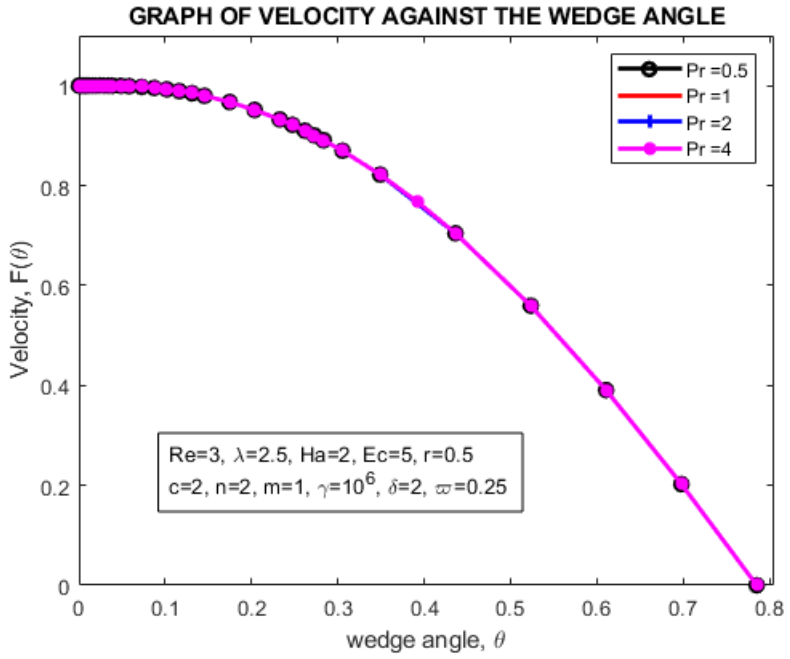

Figure 5.5: Effects of Pr on velocity profiles.

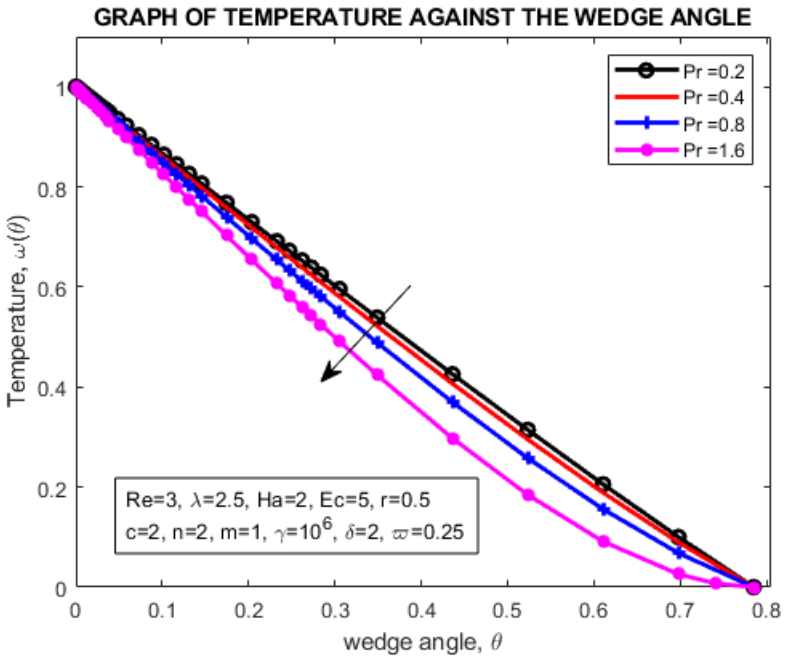

Figure 5.6: Effects of Pr on temperature profiles.

It is noted from Figure 5.5 that an increase in Prandtl number does not result in a significant change in the fluid velocity. This is due to the fact that the changes in Prandtl number are sufficiently small to cause significant change in fluid velocity. It is noted from Figure 5.6 that an increase in Prandtl number decreases the fluid temperature. This is because an increase in the Prandtl number means that the thermal diffusivity is less predominant. The high thermal radiation consequently results in a decrease in the fluid temperature.

5.5 Effects of Varying Eckert number on Velocity and Temperature Profiles

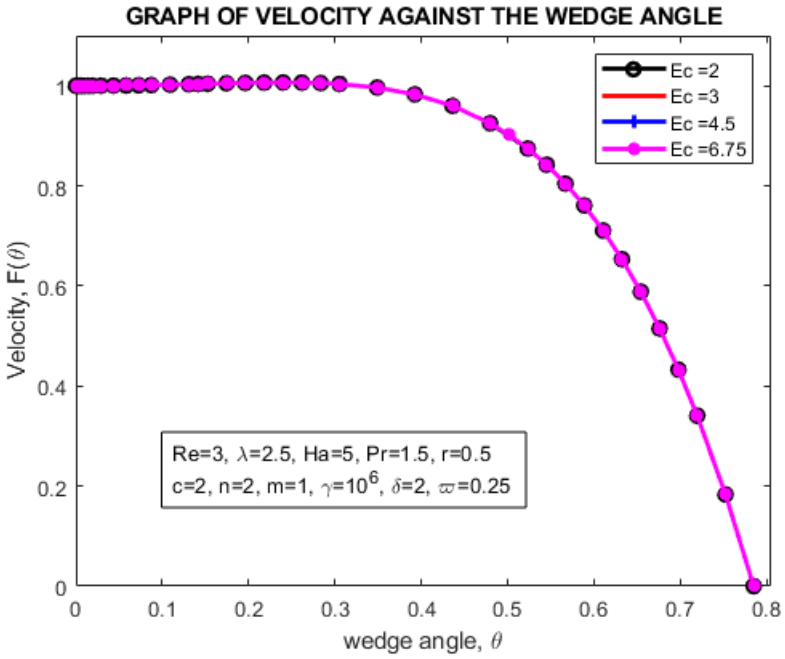

Figure 5.7: Effects of Ec on velocity profiles.

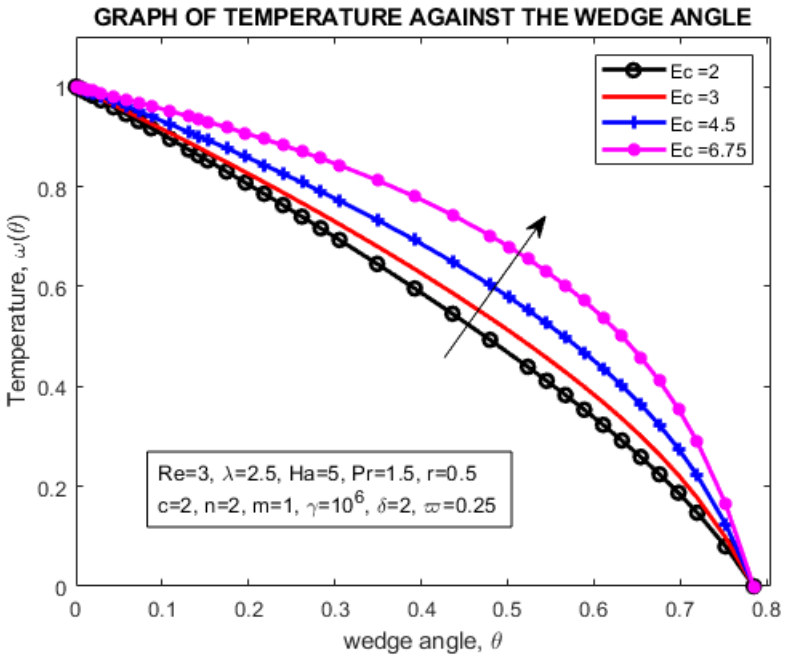

Figure 5.8: Effects of Ec on temperature profiles.

It is noted from Figure 5.7 that an increase in Eckert number doesn't lead to a significant change in the fluid velocity. This is due to the fact that the changes in Eckert number are sufficiently small to cause significant change in fluid velocity. It is noted from Figure 5.8 that an increase in Eckert number increases the fluid temperature. This is because increasing the Eckert number allows more energy to be stored in the fluid region, causing the temperature within the fluid to greatly increase. This is significant in high-temperature processes such as polymer processing.

5.6 Effects of Varying the Unsteadiness Parameter on Velocity and Temperature Profiles

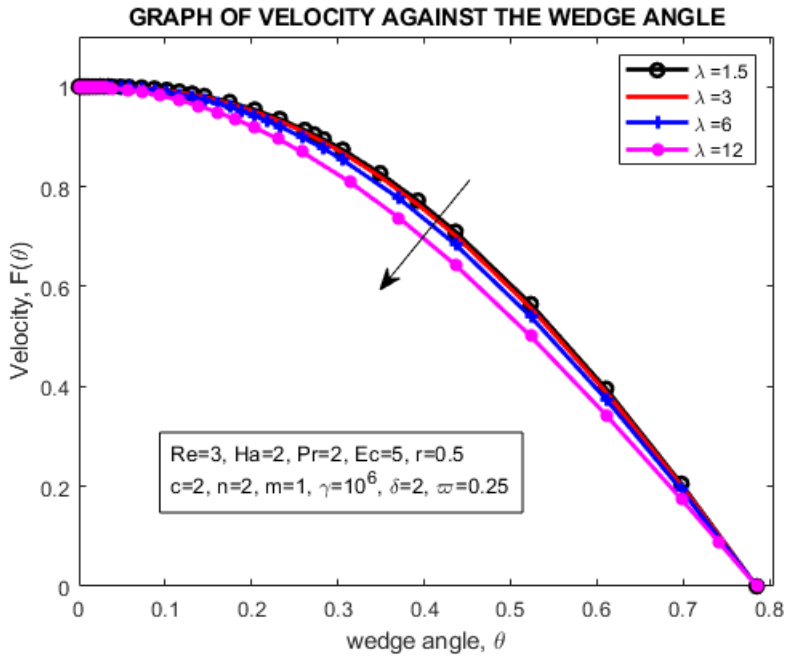

Figure 5.9: Effects of λ on velocity profiles.

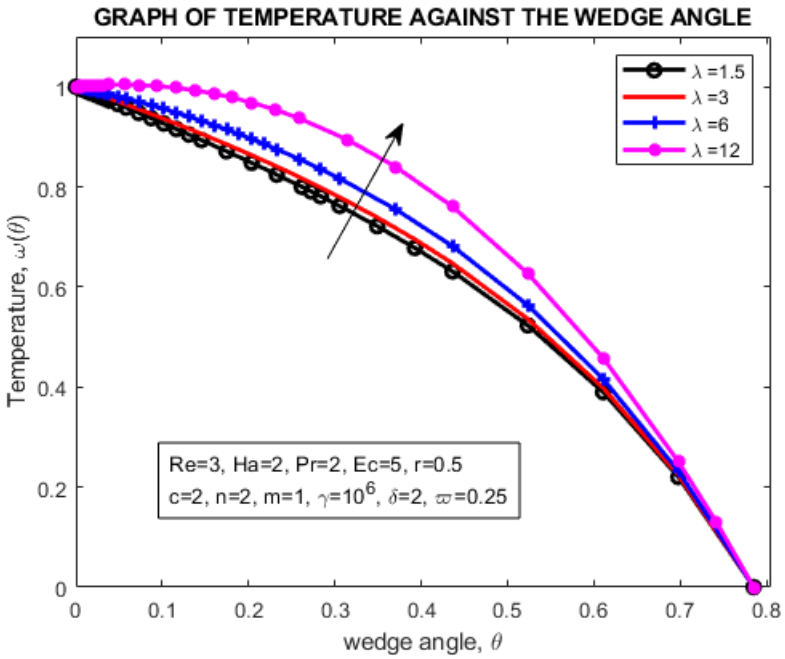

Figure 5.10: Effects of λ on temperature profiles.

It is noted from Figure 5.9 that an increase in the values of the unsteadiness parameter decreases the fluid velocity. This is because an increase in the unsteadiness parameter implies that the boundary tends to be nearer to the centerline. So, the presence of the frictional force increases the drag between the boundary and the fluid particles and as a result, forming a boundary layer which extends into the flow region. Hence, this retards the transport phenomenon.

It is noted from Figure 5.10 that an increase in the values of the unsteadiness parameter increases the fluid temperature. This is due to the fact that there is viscous dissipation taking place in the fluid as it flows (i.e., the fluid viscosity takes kinetic energy from the motion of the fluid and converts it into heat). This heats up the fluid and so as time increases, the system acquires more heat and hence increasing the fluid temperature.

5.7 Effect of parameter variations on skin-friction coefficient and rate of heat transfer

The quantities of practical interest in this study are the skin-friction coefficient and the rate of heat transfer. The local skin-friction coefficient and the local Nusselt number which are respectively proportional to $-F'(0)$ and $-\omega'(0)$ are computed and their numerical values tabulated below.

Table 5.1: Skin-friction coefficient and rate of heat transfer for various values of the parameters Re, Ha, Pr, Ec, and λ

Re	Ha	Pr	Ec	λ	C_f	N_u
3	3	2	5	2.5	1.0745×10^{-8}	0.8822
6	3	2	5	2.5	5.5941×10^{-9}	1.2001
12	3	2	5	2.5	2.5897×10^{-9}	1.5872
24	3	2	5	2.5	4.8740×10^{-9}	2.0214
3	0.5	2	5	2.5	-79.9781	1.5626
3	1	2	5	2.5	-0.4556	1.3985
3	2	2	5	2.5	3.9206×10^{-7}	1.0894
3	4	2	5	2.5	4.0219×10^{-9}	0.7472
3	2	0.5	5	2.5	3.9196×10^{-7}	1.9359
3	2	1	5	2.5	3.9196×10^{-7}	1.6602
3	2	2	5	2.5	3.9196×10^{-7}	1.0894
3	2	4	5	2.5	3.9196×10^{-7}	-0.1360
3	2	1.5	2	2.5	8.2165×10^{-5}	1.6165
3	2	1.5	3	2.5	8.2165×10^{-5}	1.4303
3	2	1.5	4.5	2.5	8.2165×10^{-5}	1.1512
3	2	1.5	6.75	2.5	8.2165×10^{-5}	0.7324
3	2	2	5	1.5	2.9528×10^{-7}	1.2175
3	2	2	5	3	4.5260×10^{-7}	1.0244
3	2	2	5	6	1.0747×10^{-6}	0.6200
3	2	2	5	12	-4.6420×10^{-8}	-0.2733

The results of varying the Reynolds number, Hartmann number, Prandtl number, Eckert number, and unsteadiness parameter on the local skin-friction coefficient and the local Nusselt number are shown in Table 5.1. It is noted that the skin-friction coefficient increases with increasing values of the unsteadiness parameter. This is due to the formation and extension of the boundary layer into the flow region which retards the motion of the fluid. The skin-friction coefficient decreases with increasing values of the Reynolds number and Hartmann number. This is due to the fact that skin friction slows moving things down and needs a constant energy supply to be overcome. The more friction, the more energy has to be supplied, and this energy is lost as heat. Further, large Reynolds

number signifies lower viscosity −this means that a large Reynolds number always results in lower friction. It is noted further that the skin-friction coefficient remains constant with increasing values of the Prandtl number and Eckert number. This is due to the fact that the changes in both Prandtl number and Eckert number are sufficiently small to cause significant change in skin-friction coefficient.

Also, it is noted that the rate of heat transfer increases with increase in Reynolds number. This is because Reynolds number is directly proportional to the Nusselt number thus an in crease in Reynolds number enhances the rate of heat transfer. It is noted further that the rate of heat transfer decreases with increase in Hartmann number, Prandtl number, Eckert number, and unsteadiness parameter. This is because increase in Ha, Pr, Ec and λ lead to increase in the fluid temperature. Since the Nusselt number is directly proportional to the negative of the temperature gradient, an in crease in Ha, Pr, Ec and λ consequently increase the rate of heat transfer.

The next chapter presents the conclusions of this study and recommendations for future studies which aim to extend the present study.

Chapter 6

Conclusions and Recommendations

6.1 Conclusions

The unsteady Jeffery-Hamel flow of an incompressible non-Newtonian fluid with nonlinear viscosity and skin-friction in the presence of an applied magnetic field in the direction perpendicular to the fluid motion has been studied. The corresponding model has been solved using the collocation method and simulated using MATLAB with the help of the inbuilt function called bvp4c. The effect of flow parameters on the flow variables for a conductive fluid inside a divergent wedge-shaped has been determined. Further, the skin-friction coefficient and the rate of heat transfer have been computed. From the results obtained, the following major conclusions have been drawn regarding the MHD Jeffery-Hamel unsteady flow.

(i) The fluid velocity increases with an increase in Reynolds number. The velocity, however, decreases with an increase in Hartmann number and unsteadiness parameter.

(ii) The fluid temperature increases with an increase in Reynolds number, Hartmann number, Eckert number, and unsteadiness parameter. It, however, decreases with an increase in Prandtl number.

(iii) The skin-friction coefficient increases with an increase in the unsteadiness parameter. The skin-friction coefficient, however, decreases with an increase in Reynolds number and Hartmann number. The skin-friction coefficient is very important for engineers since it enables them to determine the material (or coating) to use in order to construct materials which preserve energy.

(iv) The rate of heat transfer increases with an increase in Reynolds number. It, however, decreases with an increase in Hartmann number, Prandtl number, Eckert number, and unsteadiness parameter.

The results obtained from the present study can be used to complement and/or supplement the ongoing magnetic drug targeting research which considers non-Newtonian fluid such as ferrofluid.

In particular, the results of varying the viscous dissipation parameter (Eckert number) are useful in high-temperature processes such as polymer processing.

6.2 Recommendations

The present study is a significant contribution to the study of the MHD Jeffry-Hamel unsteady flow of an incompressible non-Newtonian fluid and heat transfer. The study of the effects of magnetic field on fluid flow is very important especially in duct flow problems in which the Hartmann number is of order greater than unity. However, there arise some related areas for further investigation. The following are some of the recommendations for future researchers who aim to extend this work.

(i) An extension of this study to turbulent hydromagnetic Jeffry-Hamel flow of a compressible fluid since most fluid flows of engineering interest are turbulent and compressible.

(ii) Flow involving variable magnetic field applied at an angle and variable thermal conductivity. Consider a case of fluid flowing in a convergent wedge-shaped and incorporate both Hall effect and Joule heating.

References

Ananthaswamy, V. and Yogeswari, N. (2016). A study on mhd jeffery--hamel flow in nanofluids using new homotopy analysis method. *International Journal of Scientific Research and Modern Education*, 1(1):2455--5630.

Arthur, E. M., Seini, I. Y., and Bortteir, L. B. (2015). Analysis of casson fluid flow over a vertical porous surface with chemical reaction in the presence of magnetic field. *Journal of Applied Mathematics and Physics*, 3(06):713.

Batchelor, G. K. (2000). *An introduction to fluid dynamics*. Cambridge university press.

Domairry, D. G., Mohsenzadeh, A., and Famouri, M. (2009). The application of homotopy analysis method to solve nonlinear differential equation governing jeffery--hamel flow. *Communications in Nonlinear Science and Numerical Simulation*, 14(1):85--95.

Hale, N. P. (2006). A sixth-order extension to the matlab bvp4c software of j. kierzenka and l. shampine. *Department of Mathematics, Imperial College London*.

Hamel, G. (1917). Spiralförmige bewegungen zäher flüssigkeiten. *Jahresbericht der deutschen mathematiker-vereinigung*, 25:34--60.

Hasanpour, A., Omran, M. P., Ashorynejad, H. R., Ganji, D. D., Hussein, A. K., and Moheimani, R. (2011). Investigation of heat and mass transfer of mhd flow over the movable permeable plumb surface using ham. *Middle-East Journal of Scientific Research*, 9(4):510--515.

Imani, A. A., Rostamian, Y., Ganji, D. D., and Rokni, H. B. (2012). Analytical investigation of jeffery-hamel flow with high magnetic field and nano particle by rvim. *International Journal of Engineering*, 25(3):249--256.

Jeffery, G. B. (1915). L. the two-dimensional steady motion of a viscous fluid. *The London, Edinburgh, and Dublin Philosophical Magazine and Journal of Science*, 29(172):455--465.

Khan, U., Ahmed, N., Sikandar, W., and Mohyud-Din, S. T. (2016). Jeffery hamel flow of a non-newtonian fluid. *Journal of Applied and Computational Mechanics*, 2(1):21--28.

Khan, U., Ahmed, N., Zaidi, Z., Jan, S., and Mohyud-Din, S. T. (2013). On jeffery--hamel flows. *International Journal of Modern Mathematical Science*, 7:236--247.

Kierzenka, J. and Shampine, L. F. (2001). A bvp solver based on residual control and the maltab pse. *ACM Transactions on Mathematical Software (TOMS)*, 27(3):299--316.

Manyonge, W., Kiema, D., and Iyaya, C. (2012). Steady mhd poiseuille flow between two infinite parallel porous plates in an inclined magnetic field. *International Journal of Pure and Applied Mathematics*, 76(5):661--668.

Mohyud-Din, S. T., Khan, U., and Hassan, S. M. (2016). Numerical investigation of magnetohydrodynamic flow and heat transfer of copper--water nanofluid in a channel with non-parallel walls considering different shapes of nanoparticles. *Advances in Mechanical Engineering*, 8(3):1687814016637318.

Mukhopadhyay, S. (2012). Heat transfer analysis of the unsteady flow of a maxwell fluid over a stretching surface in the presence of a heat source/sink. *Chinese Physics Letters*, 29(5):054703.

Mukhopadhyay, S., De, P. R., Bhattacharyya, K., and Layek, G. (2013). Casson fluid flow over an unsteady stretching surface. *Ain Shams Engineering Journal*, 4(4):933--938.

Mutua, N. (2013). *Stokes problem of a convective flow past a vertical infinite plate in a rotating system in presence of variable magnetic field*. PhD thesis.

Nagler, J. (2017). Jeffery-hamel flow of non-newtonian fluid with nonlinear viscosity and wall friction. *Applied Mathematics and Mechanics*, 38(6):815--830.

Nguyen, Q.-H. and Nguyen, N.-D. (2012). Incompressible non-newtonian fluid flows. In *Continuum Mechanics-Progress in fundamentals and Engineering applications*. InTech.

Pavithra, G. M. and Gireesha, B. J. (2014). Unsteady flow and heat transfer of a fluid-particle suspension over an exponentially stretching sheet. *Ain Shams Engineering Journal*, 5(2):613--624.

Petroudi, I. R., Ganji, D., Nejad, M. K., Rahimi, J., Rahimi, E., and Rahimifar, A. (2014). Transverse magnetic field on jeffery--hamel problem with cu--water nanofluid between two non parallel plane walls by using collocation method. *Case Studies in Thermal Engineering*, 4:193--201.

Poor, H. Z., Moosavi, H., Moradi, A., and Parastarfeizabadi, M. (2014). On thermal radiation effect in the mhd jeffery--hamel flow of a second grade fluid. *International Journal for Research in Applied Science and Engineering Technology*, 2(vii):219--233.

Pramanik, S. (2014). Casson fluid flow and heat transfer past an exponentially porous stretching surface in presence of thermal radiation. *Ain Shams Engineering Journal*, 5(1):205--212.

Rahman, A. M., Alamb, M. S., and Uddinc, M. J. (2016). Influence of magnetic field and thermophoresis on transient forced convective heat and mass transfer flow along a porous wedge with variable thermal conductivity and variable prandtl number. *International Journal of Advances in Applied Mathematics and Mechanics*, 3(4):49--64.

Rostami, A., Akbari, M., Ganji, D., and Heydari, S. (2014). Investigating jeffery-hamel flow with high magnetic field and nanoparticle by hpm and agm. *Open Engineering*, 4(4):357--370.

Salih, A. (2011). Conservation equations of fluid dynamics.

Shah, Z., Gul, T., Khan, A. M., Ali, I., Islam, S., and Husain, F. (2017). Effects of hall current on steady three dimensional non-newtonian nanofluid in a rotating frame with brownian motion and thermophoresis effects. *Journal of Engineering and Technology*, 6:280--296.

Sheikholeslami, M., Mollabasi, H., and Ganji, D. (2015). Analytical investigation of mhd jeffery--hamel nanofluid flow in non-parallel walls. *International Journal of Nanoscience and Nanotechnology*, 11(4):241--248.

Yang, C. (2008). A study of electrical properties in bismuth thin films. *Research Project (on the Internet) in Research Experiences for Undergraduates, Materials Physics, Florida University*.

APPENDICES

A.1 Publication

Part of this work has been published in the Global Journal of Pure and Applied Mathematics as follows:

[1] Ochieng, F. O., Kinyanjui, M. N., & Kimathi, M. E. (2018). Hydromagnetic Jeffery-Hamel Unsteady Flow of a Dissipative Non-Newtonian Fluid with Nonlinear Viscosity and Skin Friction. *Global Journal of Pure and Applied Mathematics, 14*(8), 1101-1119. https://www.ripublication.com/gjpam18/gjpamv14n8_07.pdf

A.2 MatLab Codes

A.2.1 Code for varying the Reynolds number

```
%-------------------------------------------------------------------------
% This code generates the velocity and temperature profiles together with
% the skin-friction coefficient and rate of heat transfer when the Reynolds
% number is varied.
%-------------------------------------------------------------------------
%   The model equations are first reduced to a system of first order ODEs
%   as follows:
%   Let y(1)=F, y(2)=F', y(3)=F'', y(4)=w, and y(5)=w'
%   =>  dy(1)=y(2), dy(2)=y(3), dy(3)=F''', dy(4)=y(5), and dy(5)=w''
%
%   The corresponding boundary conditions are
%      ya(1) - Umax=0
%      ya(5)=0
%      ya(2)=0
%      ya(4) - delta^(m+1)=0
%      yb(2) + gamma*yb(1)=0
%      yb(4)=0
%
% The solution is computed here for different values of Re by continuation,
% i.e., the solution for one value of Re is used as guess for Re = Re*2.
%
function thesisReynold()
clear all; clc;
global Re Ha Pr Ec varpi c n m lambda gamma delta r epsilon Cf Nu Umax
Ha=3; % Hartmann number [0,4]
Pr=2;  % Prandtl number [1.5,12]
Ec=5;  % Eckert number [2,250]
lambda=2.5;  % unsteadiness parameter [0.5,10]
varpi=0.25; % wedge angle [0,pi/4]
c=2;  % Arbitrary constant which is a natural number c>1
n=2;  % Flow behaviour index n>1 (dilatant)
m=1;  % Arbitrary constant that is related to the wedge angle
gamma=10^(6); % Friction coefficient factor
delta=2; % Time dependent length scale
r=.5; % radius of the conduit
epsilon=2*m/(m+1);
Umax=1; % center-line velocity
nIter=4; % number of iterations
multiplier=2; % common ratio
ReInit=3; % initial value for Re
Re = ReInit;  % The solution is first sought for  Re = 3.
options = bvpset('RelTol',1e-4); %=bvpset('stats','on');   % place holder
solinit= bvpinit(linspace(0,pi/4,10),@initialguess); %y = linspace(x1,x2,n)
% generates n points. The spacing between the points is (x2-x1)/(n-1).
sol = bvp4c(@odeFunction,@bcFunction,solinit,options);
lines = {'k-o','r-','b-+','m-*','y-','c-','g'};
vLegend = {strcat('Re = ' , num2str(Re))} ;
tLegend = {strcat('Re = ' , num2str(Re))} ;
%% Velocity and Temperature profiles
Cf=(2*sol.y(2,2))/(sqrt(Re*(2-epsilon))); % skin friction coefficient
Nu=-sqrt(Re/(2-epsilon))*sol.y(5,2); % heat transfer rate
fprintf('For Re = %3.0i, Cf = %4.4f, Nu = %4.4f\n',Re,Cf,Nu);
figure(1)
plot(sol.x,sol.y(4,:),lines{1},'LineWidth',2);
axis([0 pi/3.9 0 1.1]);
%{
% For velocity profiles
```

```
title('GRAPH OF VELOCITY AGAINST THE WEDGE ANGLE');
xlabel('wedge angle, \theta');
ylabel('Velocity, F(\theta)');
%}
%{-
% For temperature profiles
title('GRAPH OF TEMPERATURE AGAINST THE WEDGE ANGLE');
xlabel('wedge angle, \theta');
ylabel('Temperature, \omega(\theta)');
%}
drawnow
hold on
for i=2:nIter
    Re = Re*multiplier;
    sol = bvp4c(@odeFunction,@bcFunction,sol,options);
    Cf=(2*sol.y(2,2))/(sqrt(Re*(2-epsilon))); % skin friction coefficient
    Nu=-sqrt(Re/(2-epsilon))*sol.y(5,2); % heat transfer rate
    fprintf('For Re = %3.0i, Cf = %4.4f, Nu = %4.4f\n',Re,Cf,Nu);
    plot(sol.x,sol.y(4,:),lines{i},'LineWidth',2);
    vLegend = [vLegend , strcat('Re = ' , num2str(Re))];
    drawnow
end
legend(vLegend{:});
%% first-order system of ODE for the model equations.
function dydx = odeFunction(theta,y)
velDenom=(theta^(c*(n-1)));
if(velDenom==0)
    velDenom=10^(-6);
end
tempDenom=(delta^(m+1));
dydx = [ y(2)
         y(3)
         -(c*(n-1)*(theta^(c*(n-1)-2))*(c*(n-1)-1)*y(2)+c*(n-1)*...
         (theta^(c*(n-1)-1))*(2*y(3)+4*y(1))-2*Re*(1/delta)^(m+1)*y(1)*...
         y(2)-(Ha^2)*y(2)+(m+1)*(r/delta)^(m+1)*lambda*y(2))/velDenom-4*y(2)
         y(5)
         -Pr*((m+1)*(r^(m+1))*lambda*y(4)+(Ec)*(theta^(c*(n-1)))*...
         (4*y(1)^2+y(2)^2))/tempDenom];
end
%% Boundary conditions for the model equations.
function res = bcFunction(ya,yb)
res = [ya(1) - Umax % - r*delta^(m+1) %
       %ya(5)
       ya(2)
       ya(4) - 1%- delta^(m+1)
       yb(2) + gamma*yb(1)
       yb(4)];
end
%% Initial Guess
function guess = initialguess(theta)
guess = [ 1
          1
          1
          1
          theta];
end
end
```

A.2.2 Code for varying the Hartmann number

```
%-------------------------------------------------------------------------
% This code generates the velocity and temperature profiles together with
% the skin-friction coefficient and rate of heat transfer when the Hartmann
% number is varied.
%-------------------------------------------------------------------------
%   The model equations are first reduced to a system of first order ODEs
%   as follows:
%   Let y(1)=F, y(2)=F', y(3)=F'', y(4)=w, and y(5)=w'
%   =>  dy(1)=y(2), dy(2)=y(3), dy(3)=F''', dy(4)=y(5), and dy(5)=w''
%
%   The corresponding boundary conditions are
%      ya(1) - Umax=0
%      ya(5)=0
%      ya(2)=0
%      ya(4) - delta^(m+1)=0
%      yb(2) + gamma*yb(1)=0
%      yb(4)=0
%
% The solution is computed here for different values of Ha by continuation,
% i.e., the solution for one value of Ha is used as guess for Ha = Ha*2.
%
function thesisHartmann()
clear all; clc;
global Re Ha Pr Ec varpi c n m lambda gamma delta r epsilon Cf Nu Umax
Re=3; % Reynolds number [3,25]
Pr=2;  % Prandtl number [1.5,12]
Ec=5;  % Eckert number [2,250]
lambda=2.5;  % unsteadiness parameter [0.5,10]
varpi=0.25; % wedge angle [0,pi/4]
c=2;  % Arbitrary constant which is a natural number c>1
n=2;  % Flow behaviour index n>1 (dilatant)
m=1;  % Arbitrary constant that is related to the wedge angle
gamma=10^(6); % Friction coefficient factor
delta=2; % Time dependent length scale
r=.5; % radius of the conduit
epsilon=2*m/(m+1);
Umax=1; % center-line velocity
nIter=4;
multiplier=2;
HaInit=.5;
Ha = HaInit;  % The solution is first sought for  Ha = 0.5.
options = bvpset('RelTol',1e-4); %=bvpset('stats','on');   % place holder
solinit = bvpinit(linspace(0,pi/4,10),@initialguess); %y = linspace(x1,x2,n)
% generates n points. The spacing between the points is (x2-x1)/(n-1).
sol = bvp4c(@odeFunction,@bcFunction,solinit,options);
lines = {'k-o','r-','b-+','m-*','y-','c-','g'};
vLegend = {strcat('Ha = ' , num2str(Ha))} ;
tLegend = {strcat('Ha = ' , num2str(Ha))} ;
%% Velocity and Temperature profiles
Cf=(2*sol.y(2,2))/(sqrt(Re*(2-epsilon))) % skin friction coefficient
Nu=-sqrt(Re/(2-epsilon))*sol.y(5,2); % heat transfer rate
fprintf('For Ha = %3.0i, Cf = %4.4f, Nu = %4.4f\n',Ha,Cf,Nu);
figure
plot(sol.x,sol.y(1,:),lines{1},'LineWidth',2);
axis([0 pi/3.9 0 1.1]);
%{-
% For velocity profiles
title('GRAPH OF VELOCITY AGAINST THE WEDGE ANGLE');
xlabel('wedge angle, \theta');
ylabel('Velocity, F(\theta)');
```

```
%}
%{
% For temperature profiles
title('GRAPH OF TEMPERATURE AGAINST THE WEDGE ANGLE');
xlabel('wedge angle, \theta');
ylabel('Temperature, \omega(\theta)');
%}
drawnow
hold on
for i=2:nIter
    Ha = Ha*multiplier;
    sol = bvp4c(@odeFunction,@bcFunction,sol,options);
    Cf=(2*sol.y(2,2))/(sqrt(Re*(2-epsilon))) % skin friction coefficient
    Nu=-sqrt(Re/(2-epsilon))*sol.y(5,2); % heat transfer rate
    fprintf('For Ha = %3.0i, Cf = %4.4f, Nu = %4.4f\n',Ha,Cf,Nu);
    plot(sol.x,sol.y(1,:),lines{i},'LineWidth',2);
    vLegend = [vLegend , strcat('Ha = ' , num2str(Ha))];
    drawnow
end
legend(vLegend{:});
hold off
% fprintf('Theta\t\t F(theta)\n')
% fprintf('%.2f\t\t%.6f\n',sol.x,sol.y(1,:))
 %% first-order system of ODE for the model equations.
function dydx = odeFunction(theta,y)
velDenom=(theta^(c*(n-1)));
if(velDenom==0)
    velDenom=10^(-6);
end
tempDenom=(delta^(m+1));
dydx = [ y(2)
         y(3)
         -(c*(n-1)*(theta^(c*(n-1)-2))*(c*(n-1)-1)*y(2)+c*(n-1)*...
         (theta^(c*(n-1)-1))*(2*y(3)+4*y(1))-2*Re*(1/delta)^(m+1)*y(1)*...
         y(2)-(Ha^2)*y(2)+(m+1)*(r/delta)^(m+1)*lambda*y(2))/velDenom-4*y(2)
         y(5)
         -Pr*((m+1)*(r^(m+1))*lambda*y(4)+(Ec)*(theta^(c*(n-1)))*...
         (4*y(1)^2+y(2)^2))/tempDenom];
end
%% Boundary conditions for the model equations.
function res = bcFunction(ya,yb)
res = [ya(1) - Umax % - r*delta^(m+1) %
       ya(2)
       ya(4) - 1 % - delta^(m+1)
       yb(2) + gamma*yb(1)
       yb(4)];
end
%% Initial Guess
function guess = initialguess(theta)
guess = [ 1
          1
          1
          1
          theta];
end
end
```

A.2.3 Code for varying the Prandtl number

```
%-------------------------------------------------------------------------
% This code generates the velocity and temperature profiles together with
% the skin-friction coefficient and rate of heat transfer when the Prandtl
% number is varied.
%-------------------------------------------------------------------------
%   The model equations are first reduced to a system of first order ODEs
%   as follows:
%   Let y(1)=F, y(2)=F', y(3)=F'', y(4)=w, and y(5)=w'
%   =>  dy(1)=y(2), dy(2)=y(3), dy(3)=F''', dy(4)=y(5), and dy(5)=w''
%
%   The corresponding boundary conditions are
%      ya(1) - Umax=0
%      ya(5)=0
%      ya(2)=0
%      ya(4) - delta^(m+1)=0
%      yb(2) + gamma*yb(1)=0
%      yb(4)=0
%
% The solution is computed here for different values of Re by continuation,
% i.e., the solution for one value of Pr is used as guess for Pr = Pr*2.
%
function thesisPrandtl()
clear all; clc;
global Re Ha Pr Ec varpi c n m lambda gamma delta r epsilon Cf Nu Umax
Re=3; % Reynolds number [3,25]
Ha=2; % Hartmann number [0,4]
Ec=5;  % Eckert number [2,250]
lambda=2.5;  % unsteadiness parameter [0.5,10]
varpi=0.25; % wedge angle [0,pi/4]
c=2;  % Arbitrary constant which is a natural number c>1
n=2;  % Flow behaviour index n>1 (dilatant)
m=1;  % Arbitrary constant that is related to the wedge angle
gamma=10^(6); % Friction coefficient factor
delta=2; % Time dependent length scale
r=.5; % radius of the conduit
epsilon=2*m/(m+1);
Umax=1; % center-line velocity
nIter=4;
multiplier=2;
PrInit=.2;
Pr = PrInit;  % The solution is first sought for  Pr = 0.2.
options = bvpset('RelTol',1e-4); %=bvpset('stats','on');   % place holder
solinit = bvpinit(linspace(0,pi/4,10),@initialguess); %y = linspace(x1,x2,n)
% generates n points. The spacing between the points is (x2-x1)/(n-1).
sol = bvp4c(@odeFunction,@bcFunction,solinit,options);
lines = {'k-o','r-','b-+','m-*','y-','c-','g'};
vLegend = {strcat('Pr = ' , num2str(Pr))} ;
tLegend = {strcat('Pr = ' , num2str(Pr))} ;
%% Velocity and Temperature profiles
Cf=(2*sol.y(2,2))/(sqrt(Re*(2-epsilon))); % skin friction coefficient
Nu=-sqrt(Re/(2-epsilon))*sol.y(5,2); % heat transfer
fprintf('For Pr = %3.0i, Cf = %4.4f, Nu = %4.4f\n',Pr,Cf,Nu);
figure
plot(sol.x,sol.y(1,:),lines{1},'LineWidth',2);
axis([0 pi/3.9 0 1.1]);
%{-
% For velocity profiles
title('GRAPH OF VELOCITY AGAINST THE WEDGE ANGLE');
xlabel('wedge angle, \theta');
ylabel('Velocity, F(\theta)');
```

```
%}
%{
% For temperature profiles
title('GRAPH OF TEMPERATURE AGAINST THE WEDGE ANGLE');
xlabel('wedge angle, \theta');
ylabel('Temperature, \omega(\theta)');
%}
drawnow
hold on
for i=2:nIter
    Pr = Pr*multiplier;
    sol = bvp4c(@odeFunction,@bcFunction,sol,options);
    Cf=(2*sol.y(2,2))/(sqrt(Re*(2-epsilon))); % skin friction coefficient
    Nu=-sqrt(Re/(2-epsilon))*sol.y(5,2); % heat transfer
    fprintf('For Pr = %3.0i, Cf = %4.4f, Nu = %4.4f\n',Pr,Cf,Nu);
    plot(sol.x,sol.y(1,:),lines{i},'LineWidth',2);
    vLegend = [vLegend , strcat('Pr = ' , num2str(Pr))];
    drawnow
end
legend(vLegend{:});
hold off
% fprintf('Theta\t\t F(theta)\n')
% fprintf('%.2f\t\t%.6f\n',sol.x,sol.y(1,:))
%% first-order system of ODE for the model equations.
function dydx = odeFunction(theta,y)
velDenom=(theta^(c*(n-1)));
if(velDenom==0)
    velDenom=10^(-6);
end
tempDenom=(delta^(m+1));
dydx = [ y(2)
         y(3)
         -(c*(n-1)*(theta^(c*(n-1)-2))*(c*(n-1)-1)*y(2)+c*(n-1)*...
         (theta^(c*(n-1)-1))*(2*y(3)+4*y(1))-2*Re*(1/delta)^(m+1)*y(1)*...
         y(2)-(Ha^2)*y(2)+(m+1)*(r/delta)^(m+1)*lambda*y(2))/velDenom-4*y(2)
         y(5)
         -Pr*((m+1)*(r^(m+1))*lambda*y(4)+(Ec)*(theta^(c*(n-1)))*...
         (4*y(1)^2+y(2)^2))/tempDenom];
end
%% Boundary conditions for the model equations.
function res = bcFunction(ya,yb)
res = [ya(1) - Umax % - r*delta^(m+1) %
       ya(2)
       ya(4)- 1 %- delta^(m+1)
       yb(2) + gamma*yb(1)
       yb(4)];
end
%% Initial Guess
function guess = initialguess(theta)
guess = [ 1
          1
          1
          1
          1];
end
end
```

A.2.4 Code for varying the Eckert number

```
%-------------------------------------------------------------------------
% This code generates the velocity and temperature profiles together with
% the skin-friction coefficient and rate of heat transfer when the Eckert
% number is varied.
%-------------------------------------------------------------------------
%   The model equations are first reduced to a system of first order ODEs
%   as follows:
%   Let y(1)=F, y(2)=F', y(3)=F'', y(4)=w, and y(5)=w'
%   =>  dy(1)=y(2), dy(2)=y(3), dy(3)=F''', dy(4)=y(5), and dy(5)=w''
%
%   The corresponding boundary conditions are
%      ya(1) - Umax=0
%      ya(5)=0
%      ya(2)=0
%      ya(4) - delta^(m+1)=0
%      yb(2) + gamma*yb(1)=0
%      yb(4)=0
%
% The solution is computed here for different values of Re by continuation,
% i.e., the solution for one value of Ec is used as guess for Ec = Ec*2.
%
function thesisEckert()
clear all; clc;
global Re Ha Pr Ec varpi c n m lambda gamma delta r epsilon Cf Nu Umax
Re=3; % Reynolds number [3,25]
Ha=5; % Hartmann number [0,4]
Pr=1.5;  % Prandtl number [1.5,12]
lambda=2.5;  % unsteadiness parameter [0.5,10]
varpi=0.25; % wedge angle [0,pi/4]
c=2;  % Arbitrary constant which is a natural number c>1
n=2;  % Flow behaviour index n>1 (dilatant)
m=1;  % Arbitrary constant that is related to the wedge angle
gamma=10^(6); % Friction coefficient factor
delta=2; % Time dependent length scale
r=.5; % radius of the conduit
epsilon=2*m/(m+1);
Umax=1; % center-line velocity
nIter=4;
multiplier=1.5;
EcInit=.5;
Ec = EcInit;  % The solution is first sought for  Ec =0.5 .
options = bvpset('RelTol',1e-4); %=bvpset('stats','on');   % place holder
solinit = bvpinit(linspace(0,pi/4,10),@initialguess); %y = linspace(x1,x2,n)
% generates n points. The spacing between the points is (x2-x1)/(n-1).
sol = bvp4c(@odeFunction,@bcFunction,solinit,options);
lines = {'k-o','r-','b-+','m-*','y-','c-','g'};
vLegend = {strcat('Ec = ' , num2str(Ec))} ;
tLegend = {strcat('Ec = ' , num2str(Ec))} ;
%% Velocity and Temperature profiles
Cf=(2*sol.y(2,2))/(sqrt(Re*(2-epsilon))) % skin friction coefficient
Nu=-sqrt(Re/(2-epsilon))*sol.y(5,2); % heat transfer
fprintf('For Ec= %3.0i, Cf = %4.4f, Nu = %4.4f\n',Ec,Cf,Nu);
figure
plot(sol.x,sol.y(4,:),lines{1},'LineWidth',2);
axis([0 pi/3.9 0 1.1]);
%{
% For velocity profiles
title('GRAPH OF VELOCITY AGAINST THE WEDGE ANGLE');
xlabel('wedge angle, \theta');
ylabel('Velocity, F(\theta)');
```

```
%}
%{-
% For temperature profiles
title('GRAPH OF TEMPERATURE AGAINST THE WEDGE ANGLE');
xlabel('wedge angle, \theta');
ylabel('Temperature, \omega(\theta)');
%}
drawnow
hold on
for i=2:nIter
    Ec = Ec*multiplier;
    sol = bvp4c(@odeFunction,@bcFunction,sol,options);
    Cf=(2*sol.y(2,2))/(sqrt(Re*(2-epsilon))) % skin friction coefficient
    Nu=-sqrt(Re/(2-epsilon))*sol.y(5,2); % heat transfer
    fprintf('For Ec = %3.0i, Cf = %4.4f, Nu = %4.4f\n',Ec,Cf,Nu);
    plot(sol.x,sol.y(4,:),lines{i},'LineWidth',2);
    vLegend = [vLegend , strcat('Ec = ' , num2str(Ec))];
    drawnow
end
legend(vLegend{:});
hold off
%% first-order system of ODE for the model equations.
function dydx = odeFunction(theta,y)
velDenom=(theta^(c*(n-1)));
if(velDenom==0)
    velDenom=10^(-6);
end
tempDenom=(delta^(m+1));
dydx = [ y(2)
         y(3)
         -(c*(n-1)*(theta^(c*(n-1)-2))*(c*(n-1)-1)*y(2)+c*(n-1)*...
         (theta^(c*(n-1)-1))*(2*y(3)+4*y(1))-2*Re*(1/delta)^(m+1)*y(1)*...
         y(2)-(Ha^2)*y(2)+(m+1)*(r/delta)^(m+1)*lambda*y(2))/velDenom-4*y(2)
         y(5)
         -Pr*((m+1)*(r^(m+1))*lambda*y(4)+(Ec)*(theta^(c*(n-1)))*...
         (4*y(1)^2+y(2)^2))/tempDenom];
end
%% Boundary conditions for the model equations.
function res = bcFunction(ya,yb)
res = [ya(1) - Umax % - r*delta^(m+1) %
       ya(2)
       ya(4) - 1%- delta^(m+1)
       yb(2) + gamma*yb(1)
       yb(4)];
end
%% Initial Guess
function guess = initialguess(theta)
guess = [ 1
          1
          1
          1
          1];
end
end
```

A.2.5 Code for varying the unsteadiness parameter

```
%-------------------------------------------------------------------------
% This code generates the velocity and temperature profiles together with
% the skin-friction coefficient and rate of heat transfer when the
% unsteadiness parameter is varied.
%-------------------------------------------------------------------------
%   The model equations are first reduced to a system of first order ODEs
%   as follows:
%   Let y(1)=F, y(2)=F', y(3)=F'', y(4)=w, and y(5)=w'
%   =>  dy(1)=y(2), dy(2)=y(3), dy(3)=F''', dy(4)=y(5), and dy(5)=w''
%
%   The corresponding boundary conditions are
%      ya(1) - Umax=0
%      ya(5)=0
%      ya(2)=0
%      ya(4) - delta^(m+1)=0
%      yb(2) + gamma*yb(1)=0
%      yb(4)=0
%
% The solution is computed here for different values of lambda by
% continuation, i.e., the solution for one value of lambda is used as guess
% for lambda = lambda*2.
%
function thesisLambda()
clear all; clc;
global Re Ha Pr Ec varpi c n m lambda gamma delta r epsilon Cf Nu Umax
Re=3; % Reynolds number [3,100]
Ha=2; % Hartmann number [0,4]
Pr=2;  % Prandtl number [0.5,10]
Ec=5;  % Eckert number [0,10]
varpi=.25; % wedge angle [0,pi/4]
c=2;  % Arbitrary constant which is a natural number c>1
n=2;  % Flow behaviour index n>1 (dilatant)
m=1;  % Arbitrary constant that is related to the wedge angle
gamma=10^(6); % Friction coefficient factor
delta=2; % Time dependent length scale
r=.5; % radius of the conduit
epsilon=2*m/(m+1);
Umax=1; % center-line velocity
nIter=4;
multiplier=2;
lambdaInit=1.5;
lambda= lambdaInit;  % The solution is first sought for  lambda =1.5
options = bvpset('RelTol',1e-4); %=bvpset('stats','on');   % place holder
solinit = bvpinit(linspace(0,pi/4,10),@initialguess); %y = linspace(x1,x2,n)
% generates n points. The spacing between the points is (x2-x1)/(n-1).
sol = bvp4c(@odeFunction,@bcFunction,solinit,options);
lines = {'k-o','r-','b-+','m-*','y-','c-','g'};
vLegend = {strcat('\lambda = ' , num2str(lambda))} ;
tLegend = {strcat('\lambda = ' , num2str(lambda))} ;
%% Velocity and Temperature profiles
Cf=(2*sol.y(2,2))/(sqrt(Re*(2-epsilon))) % skin friction coefficient
Nu=-sqrt(Re/(2-epsilon))*sol.y(5,2); % heat transfer
fprintf('For lambda= %3.0i, Cf = %4.4f, Nu = %4.4f\n',lambda,Cf,Nu);
figure
plot(sol.x,sol.y(1,:),lines{1},'LineWidth',2);
axis([0 pi/3.9 0 1.1]);
%{-
% For velocity profiles
title('GRAPH OF VELOCITY AGAINST THE WEDGE ANGLE');
xlabel('wedge angle, \theta');
```

```
ylabel('Velocity, F(\theta)');
%}
%{
% For temperature profiles
title('GRAPH OF TEMPERATURE AGAINST THE WEDGE ANGLE');
xlabel('wedge angle, \theta');
ylabel('Temperature, \omega(\theta)');
%}
drawnow
hold on
for i=2:nIter
    lambda = lambda*multiplier;
    sol = bvp4c(@odeFunction,@bcFunction,sol,options);
    Cf=(2*sol.y(2,2))/(sqrt(Re*(2-epsilon))) % skin friction coefficient
    Nu=-sqrt(Re/(2-epsilon))*sol.y(5,2); % heat transfer
    fprintf('For lambda = %3.0i, Cf = %4.4f, Nu = %4.4f\n',lambda,Cf,Nu);
    plot(sol.x,sol.y(1,:),lines{i},'LineWidth',2);
    vLegend = [vLegend , strcat('\lambda = ' , num2str(lambda))];
    drawnow
end
legend(vLegend{:});
hold off
%% first-order system of ODE for the model equations.
function dydx = odeFunction(theta,y)
velDenom=(theta^(c*(n-1)));
if(velDenom==0)
    velDenom=10^(-6);
end
tempDenom=(delta^(m+1));
dydx = [ y(2)
         y(3)
         -(c*(n-1)*(theta^(c*(n-1)-2))*(c*(n-1)-1)*y(2)+c*(n-1)*...
         (theta^(c*(n-1)-1))*(2*y(3)+4*y(1))-2*Re*(1/delta)^(m+1)*y(1)*...
         y(2)-(Ha^2)*y(2)+(m+1)*(r/delta)^(m+1)*lambda*y(2))/velDenom-4*y(2)
         y(5)
         -Pr*((m+1)*(r^(m+1))*lambda*y(4)+(Ec)*(theta^(c*(n-1)))*...
         (4*y(1)^2+y(2)^2))/tempDenom];
end
%% Boundary conditions for the model equations.
function res = bcFunction(ya,yb)
res = [ya(1) - Umax % - r*delta^(m+1) %
       ya(2)
       ya(4) - 1% - delta^(m+1)
       yb(2) + gamma*yb(1)
       yb(4)];
end
%% Initial Guess
function guess = initialguess(theta)
guess = [ 1
          1
          1
          1
          1];
end
end
```